1971

Spectroscopic properties and analytical applications of premixed oxygen-hydrogen flames

Nelson Vance Mossholder
Iowa State University

Spectroscopic properties and analytical applications of premixed oxygen-hydrogen flames

by

Nelson Vance Mossholder

A Dissertation Submitted to the
Graduate Faculty in Partial Fulfillment of
The Requirements for the Degree of
DOCTOR OF PHILOSOPHY

Major Subject: Analytical Chemistry

Approved:

Signature was redacted for privacy.

In Charge of Major Work

Signature was redacted for privacy.

Head of Major Department

Signature was redacted for privacy.

Dean of Graduate College

Iowa State University
Ames, Iowa

1971

TABLE OF CONTENTS

INTRODUCTION

Simple combustion flames are now one of the most useful and convenient devices available to the analytical chemist for the determination of trace concentrations of metals in solution. This usefulness stems, for the most part, from the simple manner in which a flame may convert an aerosol of a sample in solution into free atoms of the element(s) to be determined. Once free atoms are formed, they may be readily detected at the trace concentration level by their atomic absorption, emission or fluorescence spectrum.

An ideal flame for the determination of trace elements in solution should be safe, convenient, and inexpensive to operate, and should provide a temperature high enough to vaporize the sample completely, a chemical environment conducive to the atomization of all elements, and a background spectrum free from emission and absorption in the visible and ultraviolet regions. The most popular flames in the early development of analytical flame spectroscopy were those formed from premixed air-acetylene and air-hydrogen (1-7). The temperatures of these flames were high enough for many analytical requirements and their low burning velocities allowed the use of rather unsophisticated burner systems. The higher tempera-

ture surface-mixed (commonly called "turbulent" or "total consumption") oxygen-hydrogen and oxygen-acetylene flames later gained considerable popularity. These surface-mixed flames, however, possessed rather high audible and optical emission noise levels and relatively intense spectral background. Moreover, "chemical" or condensed phase solute vaporization interferences, which are particularly sensitive to aerosol particle size distribution, were found to be prevalent in these flames. Very recently, the observation that the atomization of many elements was strikingly enhanced in premixed, fuel-rich oxygen-acetylene (8) and nitrous oxide-acetylene (9-11) flames has led to extensive use of these flames, especially the latter. The premixed nitrous oxide-acetylene flame has a relatively high temperature and is capable of atomizing most elements. Free radicals in this flame, however, emit and absorb radiation in most of the visible and ultraviolet regions of the spectrum.

Several features of the premixed oxygen-hydrogen flame make it attractive as an atomization cell or excitation source in analytical spectroscopy. The emission and absorption spectra of this flame are strikingly simple and its reported temperature is only ~150^{o}K lower than that of the nitrous

oxide-acetylene flame (12). The analytical potential of this flame has, however, not been examined, apparently because burner systems which would allow both the introduction of sample aerosols and the safe combustion of the very high burning-velocity mixtures of oxygen and hydrogen have not been available. A burner especially designed (8) for the safe combustion of high burning-velocity gas mixtures has, however, provided the opportunity of experimentally evaluating the analytical utility of the premixed oxygen-hydrogen flame. This evaluation was the primary objective of this investigation.

To achieve this objective, a detailed study was made of the premixed oxygen-hydrogen flame and the behavior of elements within it. The temperature and background spectrum were examined as a function of the two most important experimental parameters, the oxidant-to-fuel ratio (O_2/H_2) and the vertical position in the flame (Ht). These data were used to interpret the emission and absorption observed for several representative elements as a function of O_2/H_2 and Ht. The comprehensive information obtained in these initial studies was then used to determine optimum analytical conditions and emission and absorption detection limits for each of the elements

examined. Finally, the premixed oxygen-hydrogen flame was compared with other commonly used flames in terms of both detection limits and solute vaporization interferences.

The primary factor that determines the analytical utility of any flame is its ability to produce free atoms from metals in solution. Quantitative experimental evaluation of the analytical potential of a flame, however, involves experimental and instrumental parameters as well as the efficiency with which metals are atomized. In order to assess the ability of the premixed oxygen-hydrogen flame to form free metal atoms, independent of experimental influences, equilibrium metal-to-metal monoxide ratios were calculated for several elements in this flame. These ratios were compared with free atom fractions previously calculated for these same elements in the nitrous oxide-acetylene flame.

EXPERIMENTAL INVESTIGATION

Review of Physical Properties

The analytical utility of any flame is ultimately determined by its physical properties. The burning velocity governs the design and operation of the burner, and the limits of inflammability define the range of chemical composition the flame may assume. More importantly, the combustion mechanism and temperature of the flame determine its atomization and excitation efficiencies, and the flame background restricts the analytically useful portion of the spectrum.

Burning velocity

The rate at which the leading edge of a flame (the "flame front") propagates is termed the burning velocity of the flame. This quantity is highly dependent upon numerous factors, particularly the nature and composition of the combustible mixture, the geometry of the burner, and the initial temperature and pressure. The burning velocity of a premixed oxygen-hydrogen flame formed from a stoichiometric mixture at an initial temperature of 300 K and burning on a cylindrical burner at a pressure of one atmosphere is 915 cm/sec (13). By comparison, the corresponding burning velocities of the premixed air-acetylene and nitrous oxide-acetylene flames are

both approximately 160 cm/sec (1).

Limits of inflammability

Combustion initiated in an oxidant-fuel mixture propagates throughout the entire mixture only if its composition (volume % fuel) falls within the limits of inflammability. These limits apparently have not been reported for mixtures containing only oxygen and hydrogen. For oxygen-hydrogen-nitrogen mixtures containing less than 3% N_2, however, the limits are approximately 9.4% and 91.6% H_2 (2).

Background spectrum

The background spectrum of oxygen-hydrogen flames consists of four components, all of which have been studied in some detail. These are: the band systems of OH and O_2, an emission continuum, and an absorption continuum. Padley (14) has attributed the emission continuum, which is responsible for the pale blue color of hydrogen flames, to the recombination of H and OH radicals:

$$H + OH \rightarrow H_2O + h\nu.$$

This continuum extends from 2000 to 6000 Å and exhibits a broad maximum at approximately 4500 Å.

The origin of the absorption continuum, which extends from below 1900 Å to approximately 2800 Å, is uncertain.

Fiorino (15) has studied the attenuation of ultraviolet radiation by the nitrous oxide-acetylene flame and Rains (16, as discussed in 15) has studied the same phenomenon in air supported propane, acetylene, and hydrogen flames. These authors found that the light transmission of their flames at wavelengths below 2500 Å varied with both the oxidant-to-fuel ratio and the site of observation in the flame.

The band spectrum of O_2 is well known (17-21). In flames, the most intense O_2 absorption bands are those in the Schumann-Runge system which extends from below 1900 Å to approximately 2500 Å. This band system arises from the electronic transition $B^3\Sigma_u^- - X^3\Sigma_g^-$. Oxygen absorption band components above ~2000 Å, however, have as their lower state excited vibrational levels within the ground electronic state. Therefore, atmospheric oxygen, at room temperature, does not absorb at wavelengths longer than 2000 Å. Oxygen emission bands are observed in the spectral region 3000-4000 Å within the oxygen-rich region of the primary reaction zones of O_2-H_2 diffusion flames (19). Even though these bands are thermally excited (19,20,22) in diffusion flames, they are generally not observed in premixed oxygen-hydrogen flames because their excitation energies are high, 6.09 eV (18), and because O_2

concentrations in premixed oxygen-hydrogen flames are relatively low.

The OH ultraviolet band system, which has been described in detail by Dieke and Crosswhite (23), is the most prominent spectral feature of all hydrogen flames in both emission and absorption (15,18-20). The major band heads of this system and the vibrational transitions involved are listed in Table 1. The high excitation energies (11.09 and 8.48 eV respectively) for the Schuler-Michel (24) and the Schuler-Woeldike (25) OH systems preclude their observation in flames.

Table 1. Identification of the bandheads of the OH ultraviolet system

Bandhead (Å)	Transition (v',v'')
2607[a]	2,0
2811	1,0
3064	0,0
3428	0,1

[a]Data in this table taken from (23).

Temperature

A meaningful interpretation of the atomic and molecular emission and absorption spectra observed in flames requires precise knowledge of the flame temperature. This requirement results from the exponential dependence of emission intensity

and many free atom formation processes upon the gas temperature (26). Several investigators have measured temperatures in oxygen-hydrogen flames, but Table 2 shows that the values obtained are so dependent upon experimental conditions that the numbers are indicative only of the range of temperatures that may be expected.

Experimental Facilities and Procedures

Optical and electronic instrumentation

The characteristics and operating conditions of the spectrometer, optical accessories and electronics are summarized in Table 3.

The importance of spatial resolution in the study of flame temperatures and atomic and molecular emission and absorption cannot be overstated. Large temperature gradients and nonuniform spatial distributions of species in the flame necessitate the examination of small, homogeneous flame volumes, if the results are to be meaningfully interpreted. By limiting both the aperture of the lens nearest the monochromator and the slit height to 2 mm, the angle of acceptance of the spectrometer and the divergence of the observed light leaving the flame were maintained at small values. Thus,

Table 2. Oxygen-hydrogen flame temperatures

Investigators	Burner type	Solution aspiration rate	Oxidant-to-fuel ratio	Position in flame	Temperature
Lurie and Sherman (27)	Premixed[a]	0 ml/min	0.50	Not stated	2933 K
Broida and Shuler (28)	Premixed[a]	0 ml/min	0.50	Reaction[b] zone	3325
				Burnt gas region	2845
Winefordner et al. (29)	Surface-mixed[c]	Not stated	0.20	Tip of inner cone	2700
			0.40	"	2750
			0.50	"	2750
			0.60	"	2630
Winefordner et al. (30)	Surface-mixed[c]	Not stated	0.50	0.8 cm	2850
				2.0 cm	2680
Gibson et al. (31)	Surface-mixed[c]	1.0 ml/min	0.25	2.0 cm	2640
Simon (32)	Surface-mixed[c]	1.7 ml/min	0.36	3.0 cm	2725

[a]Welding-torch type burners.

[b]Temperatures measured in the reaction zone are affected by a lack of equilibrium in this zone and therefore have little meaning.

[c]Beckman burners (Beckman Instruments, Fullerton, California).

Table 3. Experimental facilities and operating conditions

External optics	a 5 cm diameter, 10.8 cm focal length, fused quartz lens was used to focus a 1:1 image of the flame onto the entrance slit. This lens was diaphragmed to 2 mm when increased spatial resolution was desirable. A similar, 16.0 cm focal length lens was employed in absorption and temperature studies to form a 1:1 image of the primary source at the center of the flame.
Spectrometer	Jarrell-Ash, model 78-462, 1.0 meter Czerny-Turner scanning spectrometer with 1180 grooves/mm grating blazed for 5000 Å; effective aperture f/8.7; reciprocal linear dispersion at the exit slit is 8.2 Å/mm in the first order.
Slits	dual unilateral entrance and exit slits with straight jaws. 0 to 400 μ slit openings. The slit width was adjusted to optimize the signal-to-noise ratio for each line examined. A 2 mm slit height was used to improve spatial resolution.
Detector	S-13 response multiplier phototube, EMI 6256B.
Detector power supply	Model S-325-RM, New Jersey Electronics Corp. (500-2500V, 0-10 mA)
DC amplifier (emission studies)	Leeds and Northrup model 9836-B micro-microammeter
AC amplifier (absorption studies)	Princeton Applied Research Corp. Lock-in amplifier, model HR-8, tuned at 108 cps.

Table 3. (Continued)

Mechanical chopper (absorption studies)	Princeton Applied Research, model BZ-1, mechanical light chopper, 108 cps. modulation frequency.
Primary source (absorption studies)	Hollow cathode lamps
Recorder	Leeds and Northrup Speedomax G, model S millivolt recorder
Integrator	Infotronics Corporation, model CRS-80 with digital readout and printer
Voltage regulator	Superior Electric Company, 1 KVA automatic voltage regulator (for detector power supply, amplifiers, recorder, and integrator)

light that entered the monochromator (the solid angle of acceptance) originated in a section of the flame having dimensions at the flame center of 2mm x the slit width. Since the light is not strictly parallel, however, these dimensions are slightly larger at the ends of the flame.

Burner and nebulizer

The burner used in this study (Figure 1) was first described (8) and later modified (15) by Fiorino. A quiet, stable flame can easily be maintained on this burner, if a 7.62 cm by 0.025 cm slot is used. The burner head need

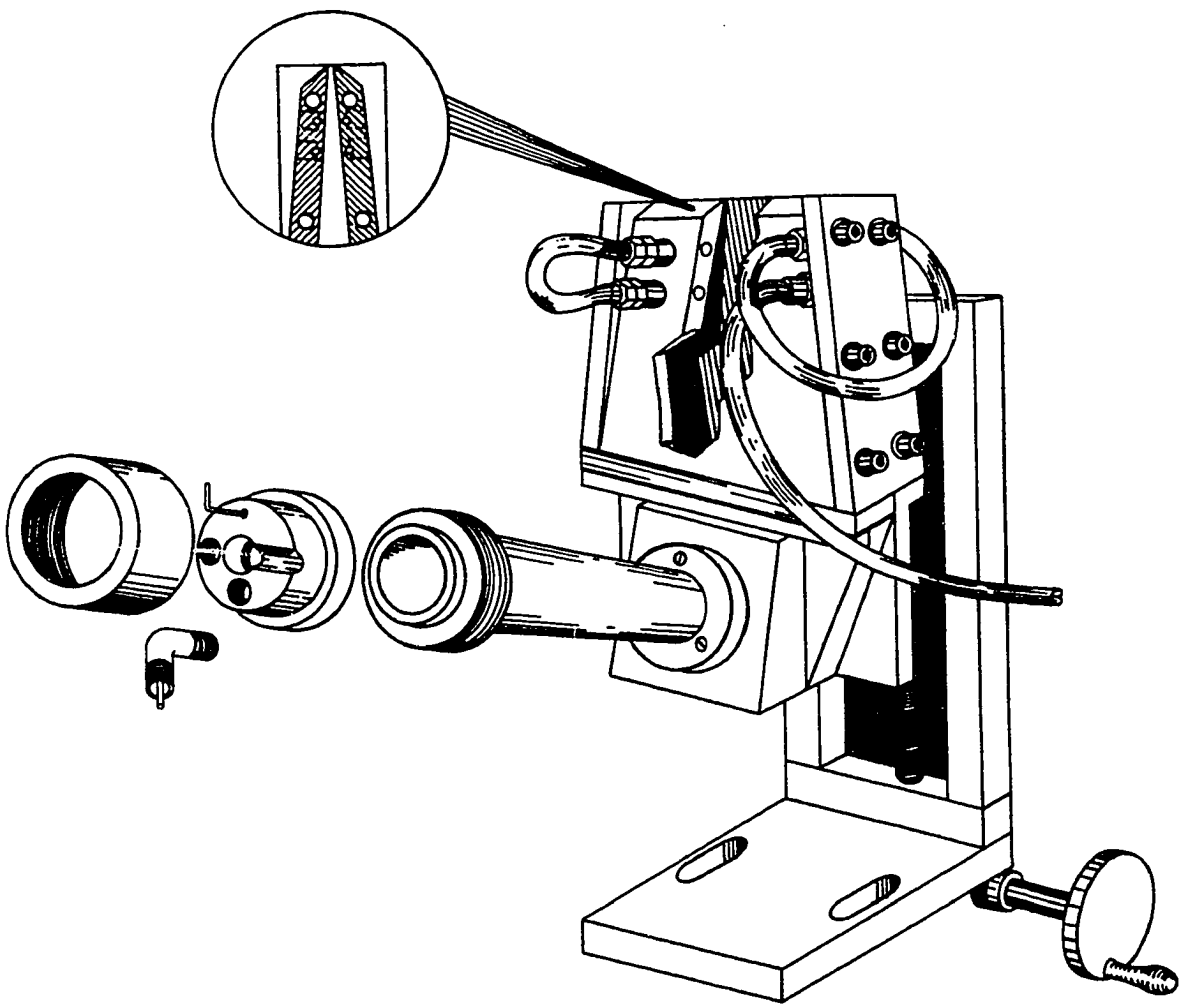

Figure 1. Cutaway view of the long path slot burner

not be cooled, even when the flame is operated for long periods of time.

Flashbacks of oxygen-hydrogen mixtures seldom occur when this burner is utilized. If the flame does flash back, the detonation is mild because the overall combustion reaction results in a reduction in the total moles of gas:

$$2H_2 + O_2 \rightarrow 2H_2O$$

The O-ring sealed, blowout plug is ejected, but no damage to the burner results.

The continuously variable nebulizer employed in this study (Varian Techtron, Walnut Creek, California), allows independent variation of the solution uptake rate (~3 ml/min) and gas flow rates, and produces an aerosol with a droplet size distribution ranging down to a few microns diameter.

Gas supply and flow metering system

Gas flows were measured with a metering system similar to the one described by Fiorino et al. (8). Unfortunately, the system employed was being used concurrently for several other studies, so that internal modifications could not be made. Instead, accessories were added to adapt it for use with oxygen and hydrogen. The flow metering system, with accessories, is diagramed in Figure 2.

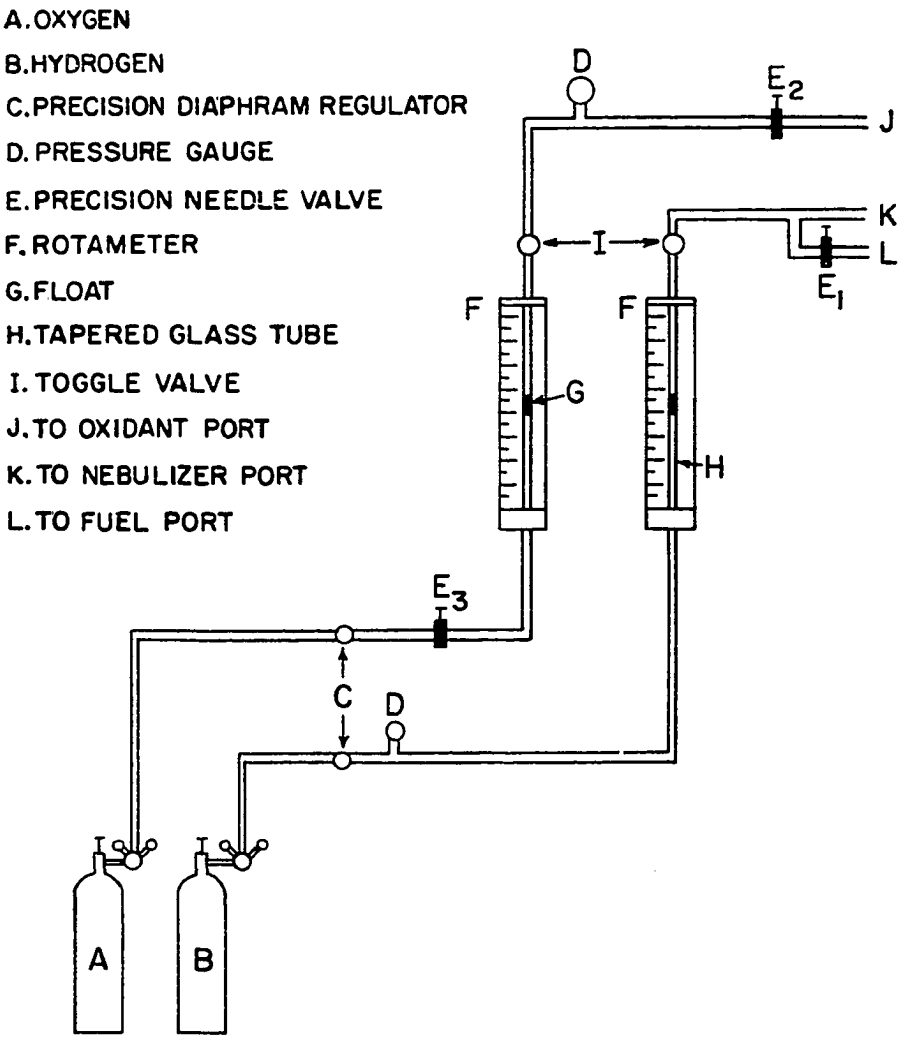

Figure 2. Gas flow regulation and metering system

The production of very fuel-rich flames required the use of extremely low oxygen flow rates. The samples were therefore nebulized by hydrogen rather than oxygen. The hydrogen flow was split into two streams; one entering the nebulizer and the other entering the burner directly. A needle valve (Mathison #100R, E_1 in Figure 2) was inserted into the auxiliary flow stream to control the total amount of hydrogen entering the burner and to maintain a relatively constant flow through the nebulizer. Minor changes in the solution uptake rate could then be corrected by adjusting the nebulizer. Since valve E_1 controlled the total hydrogen flow, the needle valve immediately preceding the rotameter (used when the fuel enters the burner directly) was opened fully, effectively removing it from the flow stream.

In the oxygen flow system, the auxiliary oxidant line in the original system was closed, and a needle valve (E_2) was inserted immediately preceding the burner. As the oxygen flow rate was changed by varying E_3, needle valve E_2 was adjusted to maintain a constant pressure within the rotameter, since the rotameters must be operated at the same constant pressure at which they were calibrated (33).

The oxygen flow system was calibrated with a precision

wet-test meter (Precision Scientific Company, Chicago, Ill.). Since the hydrogen flow rates were beyond the capacity of the wet-test meter, the hydrogen flow system was calibrated with a positive displacement gas meter (Sprague Meter Company, Bridgeport, Conn.).

In all the experiments described below, a constant total flow rate ($O_2 + H_2$) of 50 l/min was maintained. For each value of O_2/H_2 studied, the proper O_2 and H_2 flow rates were calculated, and the rotameters were adjusted accordingly. Experimental results demonstrating the need for strict maintenance of a constant total flow rate will be discussed below.

Solutions

Aqueous chloride solutions were used for all elements except Ag and Pb. $AgNO_3$ and $Pb(NO_3)_2$ as well as NaCl were dissolved directly in water and diluted to the final concentration. For the other elements, the metal or metal carbonate was dissolved in HCl. The excess acid was then removed by boiling and the final solution was prepared by diluting to the proper concentration.

Temperature measurements

The spectral line-reversal technique was used to measure temperatures in the oxygen-hydrogen flame. The principles of

this method, possible errors, and precautions which must be taken to assure reliable results have already been discussed (34-39).

A tungsten strip lamp, for which the brightness temperature is known as a function of current through the lamp, is used to measure reversal temperatures. Light from the lamp is focused on the flame and refocused, with the radiation from a strongly emitting element within the flame, onto the entrance slit of the monochromator. The lamp current is varied until no emission or absorption is observed. At this point, the brightness temperature of the lamp (the temperature of a blackbody that produces the same intensity as the lamp) at the wavelength of the spectral line of the emitting element equals the temperature of the flame.

The strip lamp was calibrated with an optical pyrometer (Leeds and Northrup, Philadelphia, Pa., model 8641), which measures the brightness temperature of the lamp at 6550 Å (T_b). It is the brightness temperature of the lamp at the wavelength of the line, however, that equals the flame temperature. The brightness temperature at 6550 Å was therefore converted to the true lamp temperature, T_{ℓ}, using Equation 1, which was derived from Wien's approximation of the blackbody

$$\frac{1}{T_b} = \frac{1}{T_\ell} - \frac{C_2}{\lambda_p} \ln (\epsilon_s \tau) \quad (1)$$

C_2 = numerical constant

λ_p = wavelength of pyrometer measurement, 6550 Å

ϵ_s = emissivity of tungsten, from (40)

τ = lens transmission factor, 0.92 (12)

radiation law and the definition of emissivity. The brightness temperature of the lamp at the wavelength of the line (the flame temperature, T_f) is then found by reinserting T_ℓ into Equation 1 with the appropriate value for λ_ℓ, the wavelength of the spectral line. Thus:

$$\frac{1}{T_f} = \frac{1}{T_\ell} - \frac{C_2}{\lambda_\ell} \ln(\epsilon_s \tau) \quad (2)$$

Temperatures measured using the spectral line reversal technique manifest the temperatures of all the atoms of the test element within the angle of acceptance of the spectrometer. Ideally, only the homogeneous temperature of the central axial flame channel is measured, but the ends and edges of the flame may also contribute unless precautions are taken to exclude them. The effects of the edges of the flame can be reduced by decreasing the size of the angle of acceptance of the spectrometer until it includes only the central

portion of the flame. Contributions from both the edges and ends of the flame can be reduced by selecting for the test element a metal that exists as free atoms only in the flame center. Metals, such as Ca, which form stable monoxides and hydroxides, are particularly suitable because they are easily oxidized by entrained air in the cool, outer portions of the flame. Ca affords two additional advantages not offered by Na, the element traditionally employed in reversal measurements. First, the resonance line of Ca (4226.7 Å) is at a considerably shorter wavelength than those of Na (5889.9 and 5895.9 Å). Equation 2 illustrates that as λ is reduced, reversal is achieved at lower values of T_ℓ and the risk of darkening the bulb by evaporating tungsten and subsequent lamp burnout is reduced. Second, the reversal pattern for the Na lines are complicated by absorption of light emitted in the hot flame center by atoms in the cooler ends of the flame (self-reversal) (41-43). Since Ca free atoms exist primarily in the flame center, the Ca line exhibits much less self-reversal. Therefore, using a restricted angle of acceptance and Ca as the test element, the temperatures measured should be those in the homogeneous, central axial channel of the flame.

Optimization of experimental conditions and data display

Several methods have been used to study the effects of changes in experimental parameters on the emission and absorption of elements observed in flames. In most flame studies, the effect of one variable at a time has been observed. For example, vertical profiles have been used to show the relationship between the emission or absorption of elements and the site of observation in the flame. The main disadvantage of this method, however, is that any interactions between two supposedly independent variables cannot be detected.

Box and Wilson (44) developed a statistical method for determining optimum experimental conditions and studying the effects of many variables. By interspersing a series of experiments with statistical calculations, the effects of k variables on the response measured are determined simultaneously, and the shape of the k+1 dimensional "response surface" is calculated. Box (45), using examples from several fields, illustrated that experiments designed using the response surface method are superior to those developed by examining a single variable at a time. Skogerboe (46) has utilized the response surface technique to study the excitation of several rare earth elements in a turbulent oxygen-hydrogen flame as a

function of oxidant-to-fuel ratio, position in the flame, and the total gas flow rate. Cellier and Stace (47) also employed this method to determine the effects of several experimental and instrumental parameters on the atomic absorption of Ca. Cellier and Stace found that the oxidant and fuel flows, the oxidant pressure and the position in the flame were the only significantly interrelated variables in their study.

The dependence of emission intensity and absorbance observed by Skogerboe and Cellier and Stace upon the flow rate and oxidant pressure resulted, in part, from the dependence of the nebulization systems they used upon these parameters. In this study, the effects of gas pressure and flow rate were minimized by using a nebulization system which was relatively independent of these variables. Even when nebulization effects were eliminated, however, the total flow rate determined the final flame volume and thus the amount of sample dilution.

As discussed below, the lowest total flow rate commensurate with safe operation of the burner produced the maximal sample concentration in the flame. Thus, by maintaining the total gas flow rate at this level, only two experimental parameters were important in the experiments described below,

the oxidant-to-fuel ratio and the flame site at which the measurement was made.

When the dependence of the desired response can be limited to two variables, it is often simpler to determine the shape of the response surface solely by experiment, thereby avoiding the somewhat involved statistical calculations. Malakoff et al. (48) employed oblique projections of three dimensional response surfaces determined entirely by experiment to illustrate the interdependence of absorbance, metal concentration and a third variable (burner position, lamp current, etc.) in atomic absorption measurements. Skogerboe et al. (49), on the other hand, projected a three dimensional response surface onto the independent variable plane to show the dependence of vanadium emission on the oxidant-to-fuel ratio and observation site in a turbulent oxygen-hydrogen flame. These contour plots convey the same information as the oblique projections of Malakoff et al. in a way that makes interpretation of the data much easier.

Response surfaces similar to those of Skogerboe et al. are employed throughout the discussion that follows to illustrate and interpret the flame temperature and the emission and absorption of species in the premixed oxygen-hydrogen flame.

The response of temperature (K), emission intensity, or absorbance is plotted against both O_2/H_2, the molar oxidant-to-fuel flow ratio (abscissa) and Ht, the vertical position in the flame (ordinate) and points of equal response are connected with lines. The point of maximum response is represented by +. Emission intensities and absorbances are normalized with respect to the maximum value to facilitate the comparison of one element with another.

The response surfaces were constructed by measuring the background correction emission intensity, absorbance, or temperature at 44 evenly spaced values of O_2/H_2 and Ht. Using electronic data processing, the corresponding response at each point was then calculated. For the emission and absorbance response surfaces, the resulting points were plotted by the computer in seven groups, each with a different symbol. The points in each group comprised a given range of relative intensities or absorbances, i.e. 1-10%, 10-25%, 25-40%, 40-55%, 55-70%, 70-85%, and 85-100% of the maximum value. Finally lines were drawn by hand to separate these groups and the lines were marked with the relative intensity of the junction (1%, 10%, 25%, etc.). No experimental aids such as a motor driven burner assembly were used

in this work. The intensities and absorbance data were recorded directly from the integrator readout onto keypunch forms. The time required to construct one plot was approximately 45 minutes. The reproducibility of the hand drawn lines was good; variation in the position of a line was at most $\pm$ 3% of the maximum value.

Results and Discussion

Visual appearance

The premixed oxygen-hydrogen flame burning on a laminar-flow slot burner is acoustically quiet and very stable. The visual appearance of the flame is highly dependent upon the oxidant-to-fuel ratio as illustrated in Figure 3. The primary reaction zone of the stoichiometric flame (with respect to the gases passing through the burner) shown in the left half of this figure is blue-white in color, approximately 1 mm in height, and is formed approximately 0.5 mm from the top of the burner. The post reaction zone or "burnt gas region" is pale blue and nearly transparent. This flame is 7.6 cm long, approximately 12 cm high and less than 1 cm wide at 2 cm above the top of the burner.

As the flame is made increasingly fuel-rich, the luminosity of both zones decreases and the size of the flame

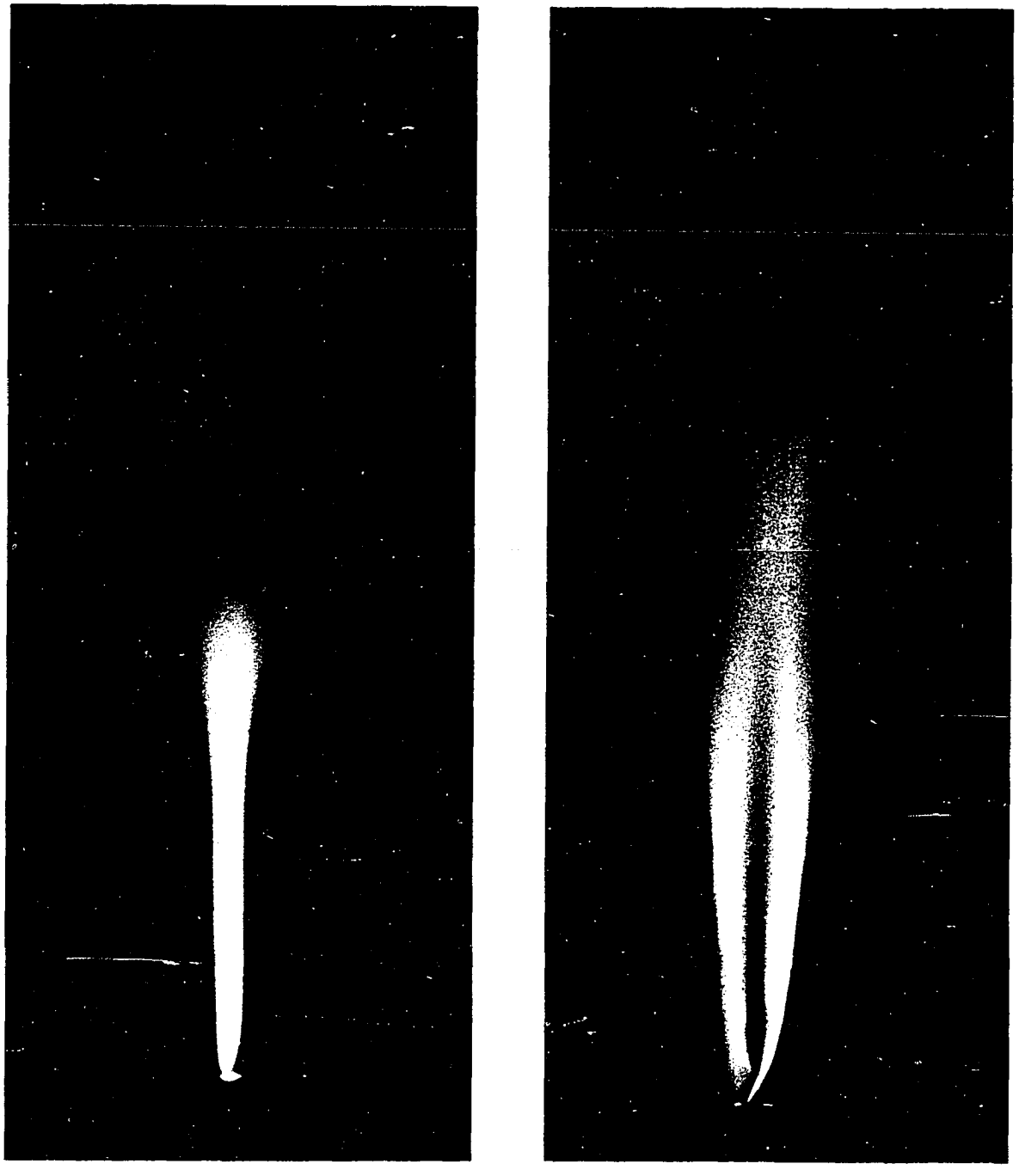

Figure 3. Photographs, taken slightly off the optical axis of the spectrometer, of the stoichiometric (left, $O_2/H_2 = 0.50$) and very fuel-rich (right, $O_2/H_2 = 0.10$) premixed oxygen-hydrogen flames

increases. At oxidant-to-fuel ratios less than 0.10, the flame is invisible in normal light, but in a darkened room the shape of the flame is that illustrated in the right half of Figure 3. When the composition of the gases leaving the burner corresponds to $O_2/H_2 \leq \sim 0.10$, the limit of inflammability is exceeded. Combustion is then supported primarily by oxygen entrained from the atmosphere, and the long primary reaction zones at the edges of the flame result. The dark central portion of the flame in this figure represents the burnt gas region. The very fuel-rich flame ($O_2/H_2 = 0.10$) is more than 20 cm high and approximately 4 cm wide at 2 cm above the burner top. The bright spot which appears near the top of the fuel-rich flame in Figure 3 is caused by Na emission from a dust particle entrained by the flame.

Temperature

The response surface of temperature in the premixed oxygen-hydrogen flame as a function of O_2/H_2 and Ht is illustrated in Figure 4, and Figure 5 shows the variation in measured horizontal temperature profiles as a function of O_2/H_2. These figures exhibit several interesting features. Of primary interest is the 2950 K maximum temperature in Figure 4, which was observed at $O_2/H_2 = 0.50$ and Ht = 0.25 cm. At this stoi-

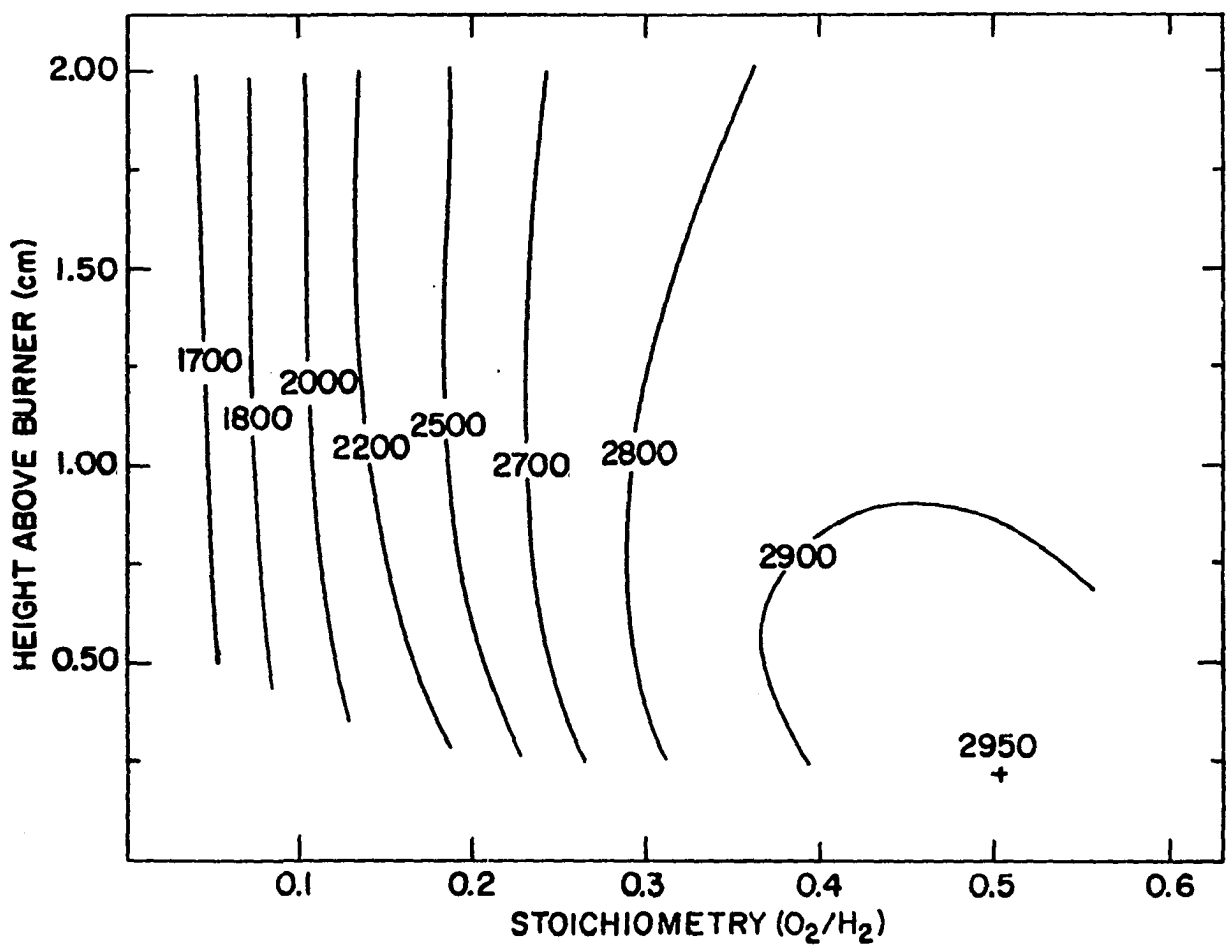

Figure 4. Response surface of temperature (K) in the premixed O_2-H_2 flame

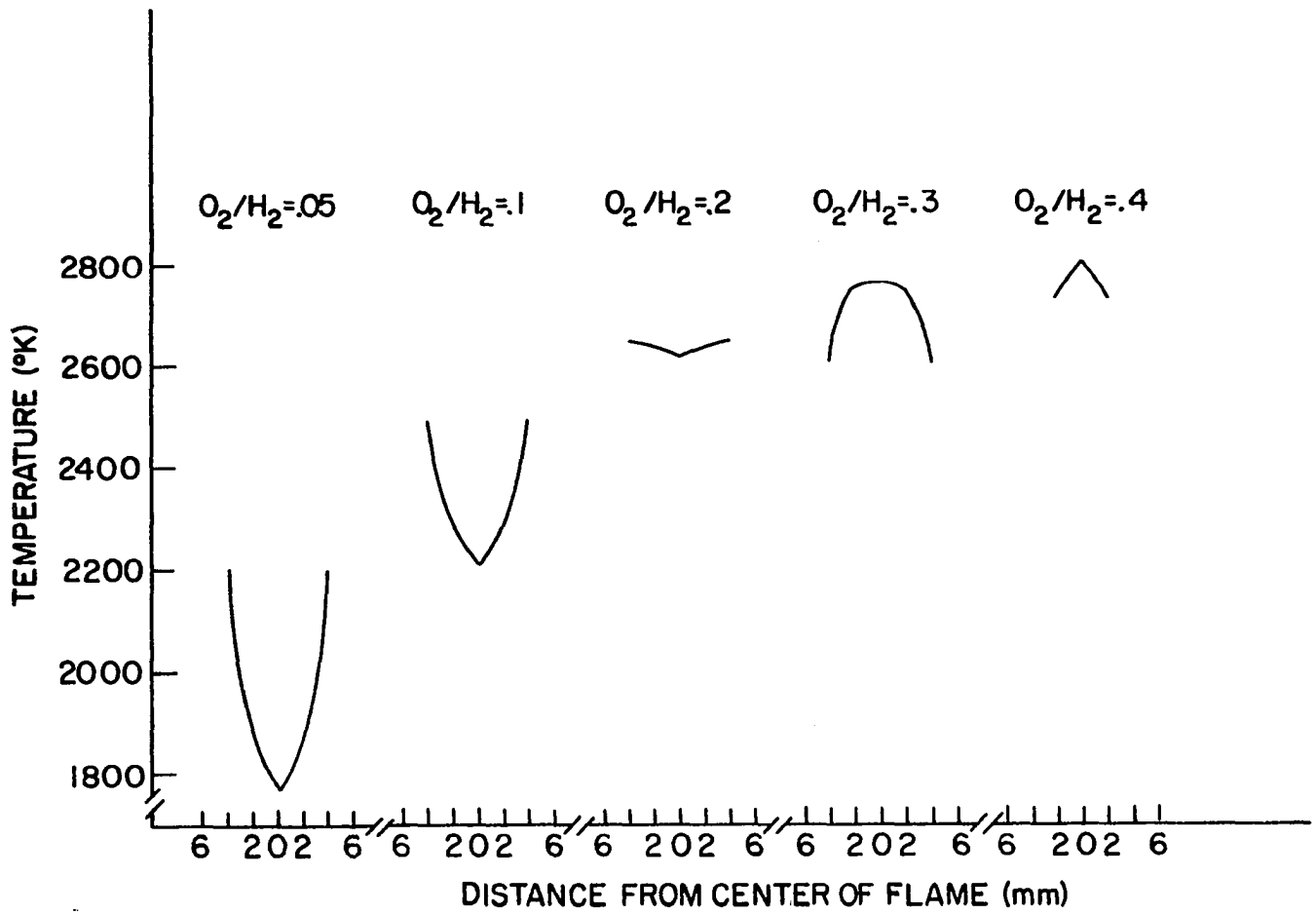

Figure 5. Horizontal temperature profiles at 2.0 cm above the burner

chiometry, the primary reaction zone, because of its small size and proximity to the burner, is outside of the angle of acceptance of the spectrometer. Thus, the nonthermal temperature distributions commonly observed in the primary reaction zone (34) could not contribute to the measured value. The maximum temperature measured in the premixed oxygen-hydrogen flame is approximately 75 K higher than the maximum temperature of the nitrous oxide-hydrogen flame (50) and less than 125 K lower than the corresponding value in the nitrous oxide-acetylene flame (12). The value 2950 K is also higher than most others reported for this flame (see Table 2) even though the flame examined in this study contained appreciable amounts of water.

Another interesting feature of the oxygen-hydrogen flame is the unusually large temperature difference (~1250 K) between the stoichiometric (O_2/H_2 = 0.50) and very fuel-rich (O_2/H_2 = 0.05) flames. Figure 4 indicates that only 150 K of this difference occurs between O_2/H_2 = 0.50 and 0.30, whereas the difference is ~600 K between O_2/H_2 = 0.30 and 0.15, and ~500 K between O_2/H_2 = 0.15 and 0.05.

The horizontal temperature profiles shown in Figure 5, as well as the response surface in Figure 4 and visual observa-

tions of the flame, support the conclusion that at oxidant-to-fuel ratios less than ~0.10 entrained atmospheric oxygen plays an important role in the combustion process. This deduction is most strongly supported by the interesting inversion of the horizontal temperature profiles. When primary oxidant (that which passes through the burner) supports the flame, the highest temperatures should be observed in the flame center, and the temperature should decrease near the edges of the flame as the entrained air dilutes and cools the flame gases. Figure 5 clearly shows this effect for O_2/H_2 = 0.30 and 0.40. As O_2/H_2 decreases from 0.20 to 0.05, there is an increasing tendency for the flame temperature to be lower in the flame center and higher near the edges of the flame. This behavior is in harmony with the existence of a diffusion flame supported primarily by atmospheric oxygen. The profiles in Figure 5 do not extend farther than 0.4 mm from the flame center because no Ca emission could be detected beyond this point.

At 0.25 cm above the burner, at all values of O_2/H_2, the flame is very narrow, so that the angle of acceptance of the spectrometer most certainly includes the edges of the flame. The effect of this on the measured temperatures is clearly

shown when Na is used as the indicating element. Since Na does not form stable oxygen-containing compounds, its free atoms should be more uniformly distributed throughout the flame than those of Ca. The comparison, in Table 4, of temperatures measured using solutions containing 500 μgCa/ml and 50 μgNa/ml clearly shows that when the flame edges are included in the angle of acceptance (at low flame heights), temperatures measured with Na are ~40 K lower than those measured using Ca. On the other hand, when the edges of the flame are excluded from the measurement (at points higher in the flame), temperatures measured using these two solutions are equal within the precision of the method (± 20 K).

Table 4. Comparison of Ca and Na reversal temperatures

O_2/H_2	Ht	T_{Ca}	T_{Na}	$T_{Ca}-T_{Na}$
0.35	0.25 cm	2850 K	2809 K	+41 K
	0.50	2833	2894	-11
	1.50	2831	2840	-9
0.40	0.25	2944	2909	+40
	0.50	2944	2926	+18
	1.00	2893	2888	+5
	1.75	2842	2847	-5
0.45	0.25	2950	2915	+35
	0.50	2944	2940	+4
	1.25	2860	2862	-2
0.55	0.25	2944	2900	+44
	0.50	2929	2930	-1
	0.75	2901	2900	+1

The effect of the ends of the flame on the measured temperatures can be illustrated by comparing temperatures determined using solutions containing several concentrations of Ca and Na. Since self-reversal becomes increasingly important at high concentrations, the contribution of the flame ends should increase as the concentration of the indicating element increases. The effect of concentration on temperatures measured using Ca and Na is illustrated in Table 5. The data in this table reveal that temperatures determined with Na are influenced by self-reversal while those determined with Ca are not, proving that the flame ends do not affect temperature measured when Ca is used as the indicating element.

Table 5. The effect of solution concentration on temperatures measured using Ca and Na as the indicating element

		Conc. (μg/ml)				
O_2/H_2	Ht(cm)	Ca	Na	T_{Ca}	T_{Na}	$T_{Ca}-T_{Na}$
0.50	0.25	500	50	2930 K	2938 K	-8 K
		2,000	200	2930	2915	+15
		10,000	1000	2930	2904	+26
	2.00	500	50	2820	2810	+10
		2,000	200	2817	2801	+16
		10,000	1000	2817	2788	+29
0.25	0.50	500	50	2700	2694	+6
		2,000	200	2700	2694	+6
		10,000	1000	2700	2690	+10
	2.00	500	50	2739	2740	-1
		2,000	200	2739	2730	+9
		10,000	1000	2739	2712	+27

Background spectrum

The background emission and absorption of flames is of interest to analytical spectroscopists because band emission and absorption often obscure the spectral lines of analytes (elements whose concentrations are to be determined). These spectral band interferences can be detected in emission by spectroscopically scanning the wavelength region containing the line of the analyte, while aspirating a blank solution into the flame. If the intensity of the interfering band component is not too high, another scan can be made while aspirating the sample solution, and the background intensity at the wavelength of the line can be subtracted from the intensity of the line plus background. The signal-to-noise ratio of the line and the precision of the measurement are both reduced when spectral interferences occur, however. In atomic absorption measurements, spectral interferences are less easily detected and cannot be corrected for because narrow line primary sources (hollow cathode lamps) are generally used, and scanning techniques cannot be employed unless a continuum primary source is used.

The analyst can often eliminate the effects of spectral interferences by choosing another line in a background free

portion of the spectrum, or by selecting experimental conditions that minimize the background emission intensity or absorbance. The avoidance of spectral interferences, however, requires detailed knowledge of the regions of the spectrum in which the flame emits and absorbs radiation, and of variations in the emission intensity and absorbance of flame bands as a function of experimental parameters.

The spectral region in which the stoichiometric, premixed oxygen-hydrogen flame emits is illustrated in Figure 6. The bands shown in this figure are all emitted by the OH radical. No emission continuum is evident in Figure 6 because a relatively low sensitivity was required to keep the OH bandhead on scale. At higher amplifications, a weak emission continuum could be observed throughout most of the spectral region illustrated. The OH bands shown in Figure 6 are also observed in absorption, as are O_2 bands and an absorption continuum which underlies the O_2 band system. The O_2 absorption bands are displayed in Figure 7, which was taken from (15).

Response surfaces of OH emission intensity and absorbance (at the 3064 Å bandhead), and the absorbance of the O_2 band component and underlying continuum at 2138.6 Å (the wavelength

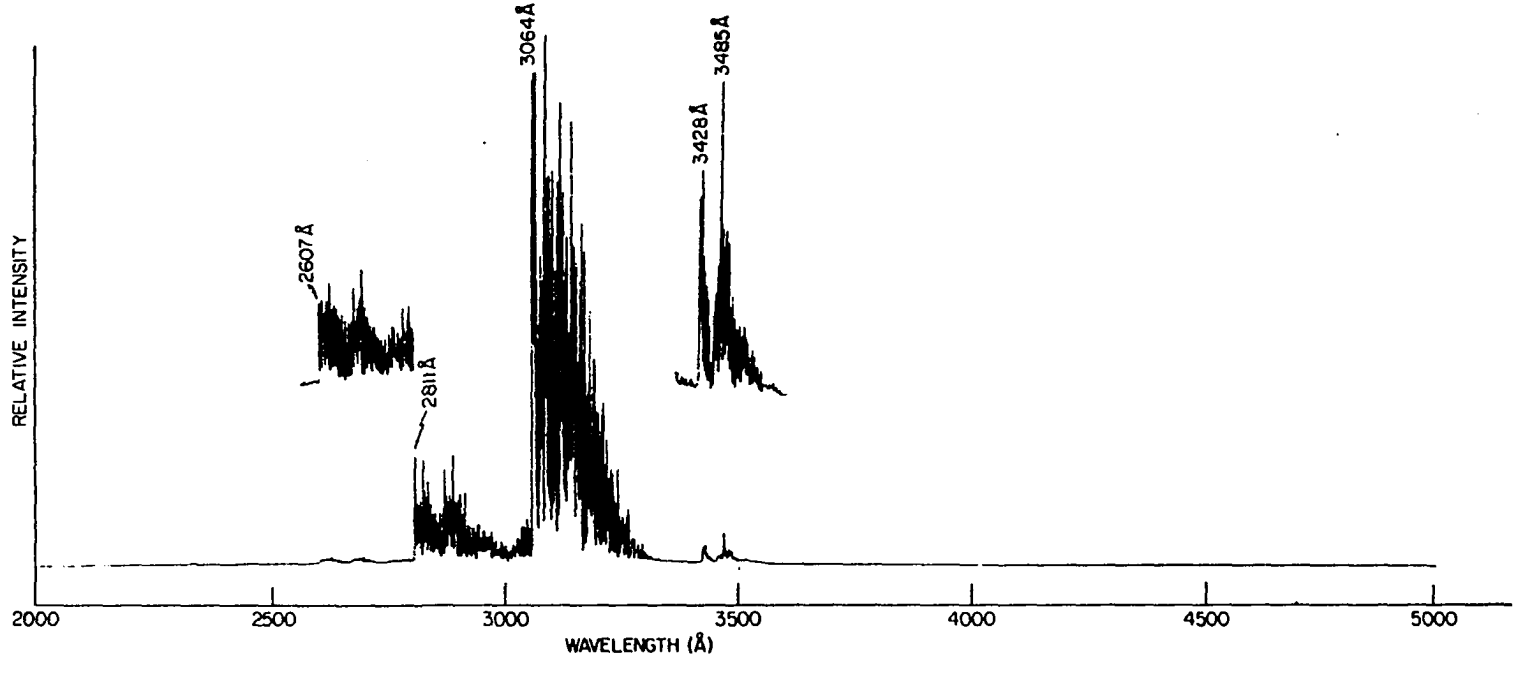

Figure 6. Emission background spectrum of the stoichiometric, premixed oxygen-hydrogen flame

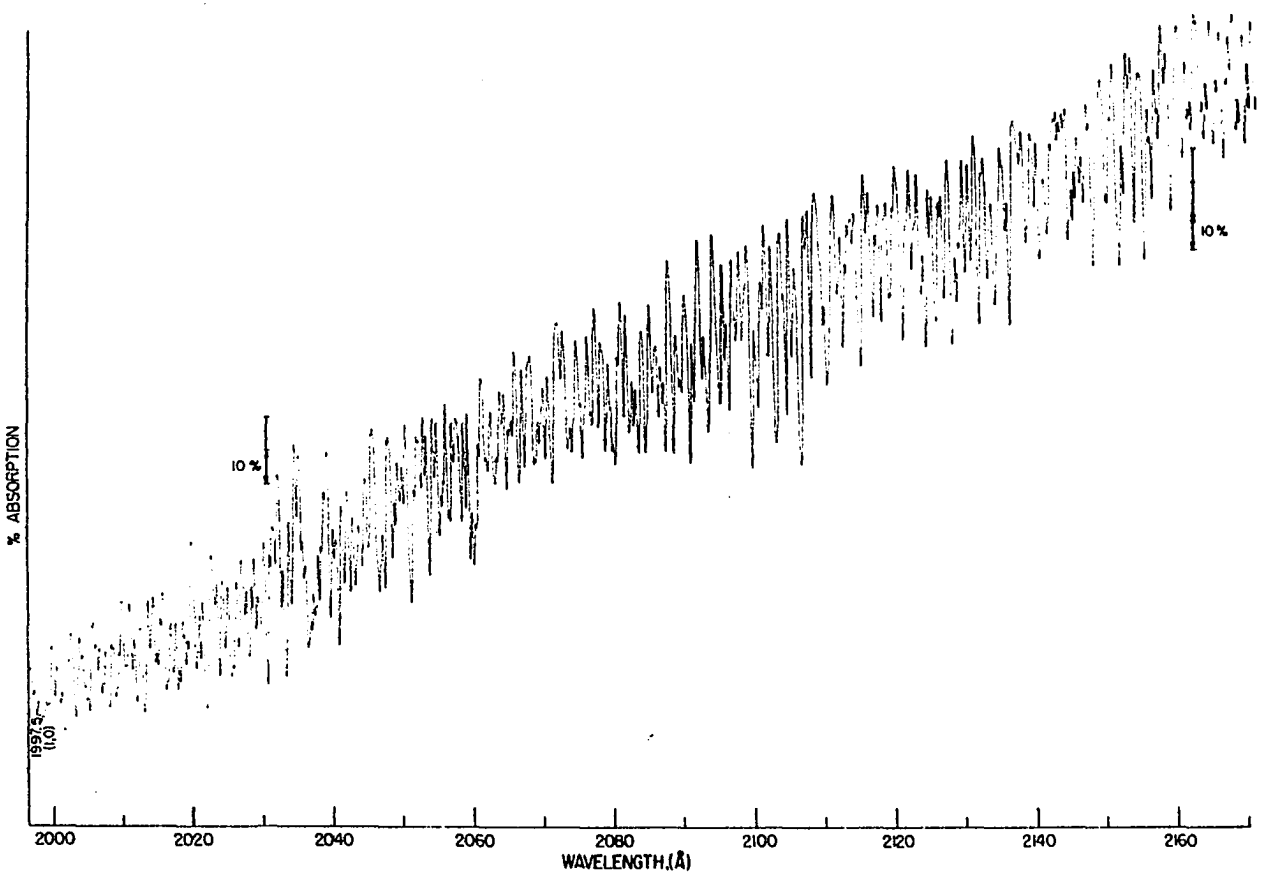

Figure 7. Absorption spectrum of O_2 in the fuel-lean, premixed oxygen-hydrogen flame, taken from (15)

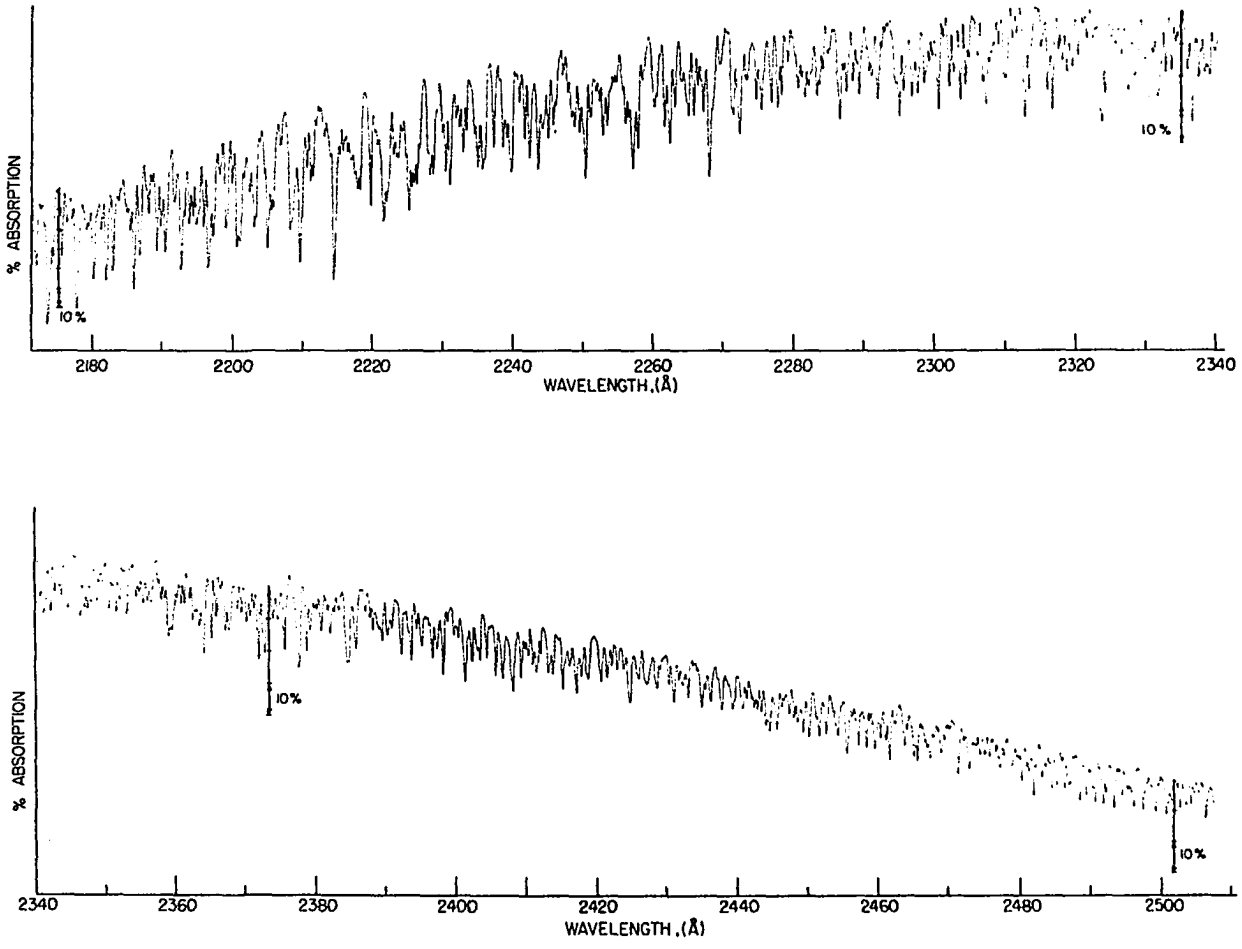

Figure 7. (Continued)

of the Zn resonance line) are found in Figures 8 and 9 respectively. The absorption response surfaces in these figures indicate the relative absorbances added to the absorbance of a spectral line in the OH and O_2 band systems as a function of O_2/H_2 and Ht. They do not, however, indicate relative changes in the concentrations of these molecules because the partition functions of OH and O_2 change significantly over the wide range of flame temperatures. In addition, the OH bandhead is comprised of several superimposed components whose relative intensities may vary with temperature.

The response surfaces in Figures 8 and 9 display several similar features. The maximum background response (emission intensity or absorbance) on all three surfaces is located 0.5 cm above the burner in a slightly fuel-lean flame (O_2/H_2 = 0.55). Furthermore, all three surfaces exhibit steadily diminishing response with decreasing O_2/H_2. This behavior reflects the reduction of the concentrations of all oxygen-containing flame species as the flame is made more fuel-rich. The drop in OH emission with decreasing oxidant-to-fuel ratio is particularly rapid, illustrating the exponential dependence of emission intensity on temperature (compare with Figure 4).

Figures 6 and 7 indicate that band emission and absorp-

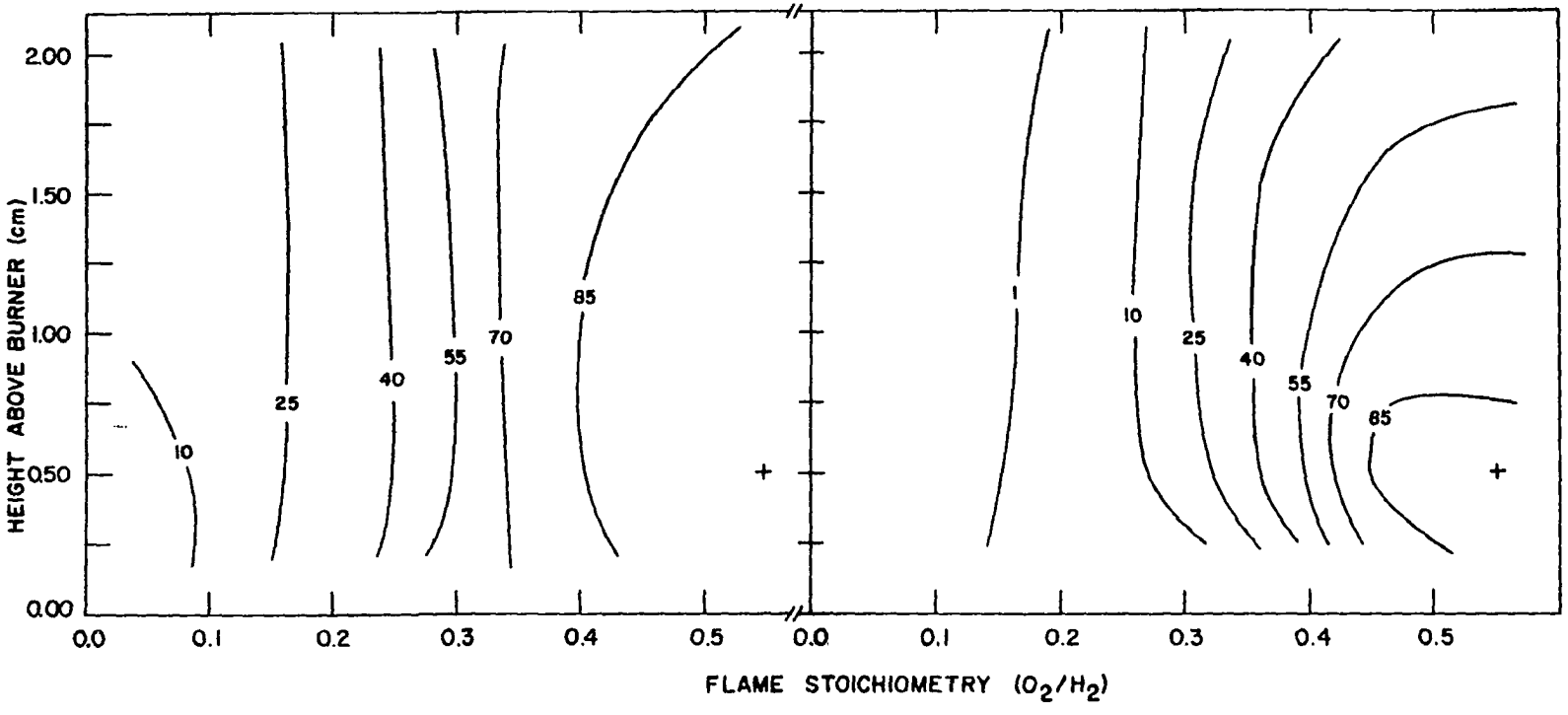

Figure 8. Response surfaces OH absorbance (left) and emission (right) in the premixed oxygen-hydrogen flame

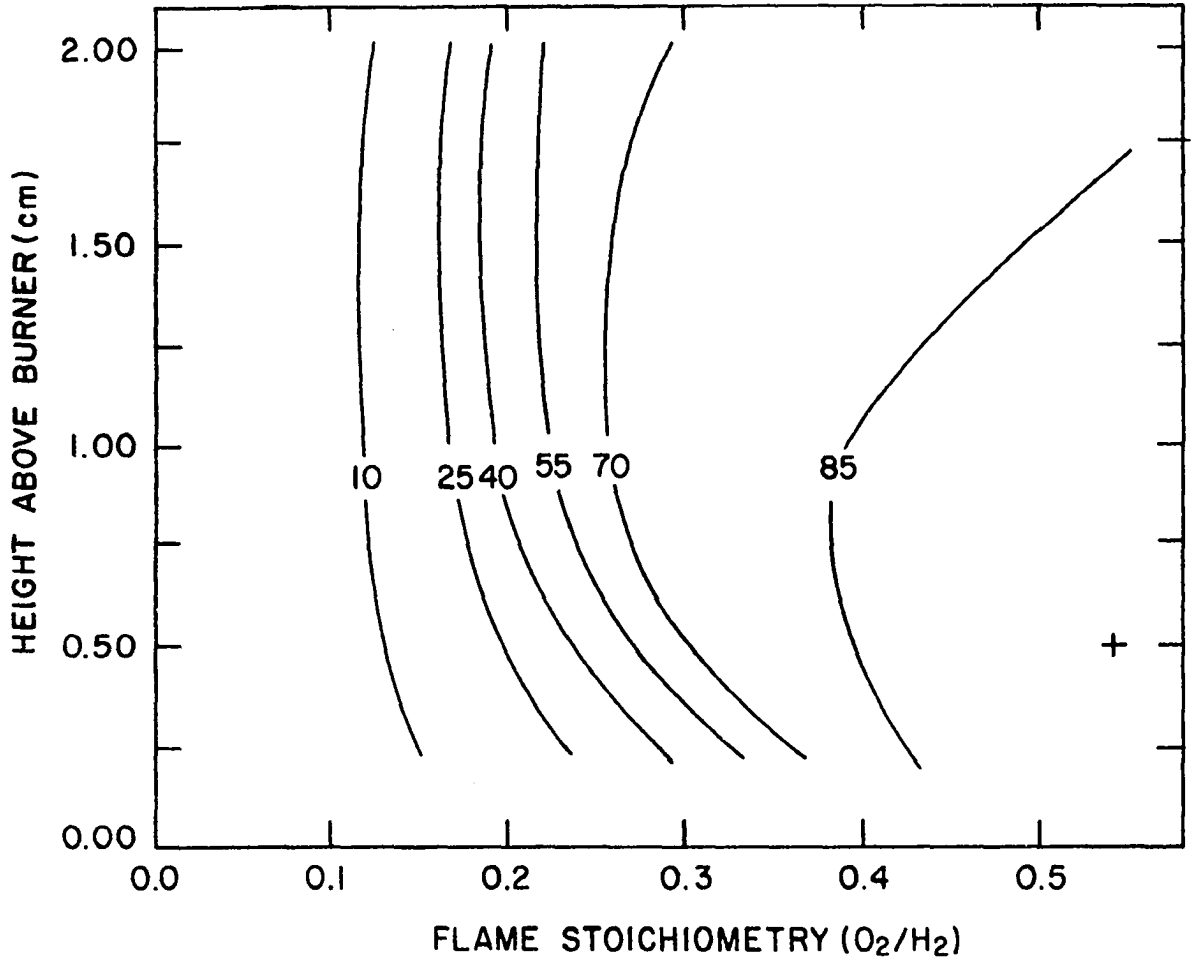

Figure 9. Response surface of flame background absorbance (O_2 band component + continuum) at 2138.6 Å

tion in the premixed oxygen-hydrogen flame is limited to the spectral region 2000- ~3500 Å. It is highly probable that the following elements, whose resonance lines (lines having as their lower state the ground state of the atom) all lie within this wavelength region, would experience spectral interference: Cd(2288.0 Å), Cu (3247.5, 3274.0 Å), Mg (2852.1 Å), Pb (2169.9, 2833.1 Å), Sn (2246.1, 2863.3 Å), and Zn (2138.6 Å). For elements such as these it is prudent to employ response surfaces similar to those in Figures 8 and 9 to select O_2/H_2 and Ht so that the background emission intensity and absorbance are minimal. Some compromise is generally necessary, however, because the experimental conditions that minimize spectral interferences produce a flame with limited atomization and excitation efficiencies as well.

Emission and absorption of representative elements

In order to study quantitatively the radiation emitted or absorbed by a species in a flame, it is necessary to determine the experimental conditions which maximize the response measured. The response surfaces of atomic absorbance and emission described below illustrate the oxidant-to-fuel ratio and observation site that produce the maximum response in each mode. These plots supply the experimental information necessary for the determination of detection limits and, in addi-

tion, provide valuable information about the free atom formation processes which occur in the premixed oxygen-hydrogen flame.

The concentration of free metal atoms in a flame can be defined in the following way:

$$\text{concentration} = \frac{\text{number of metal atoms passing through the flame/unit time}}{\text{volume of gas passing through the flame/unit time}}$$

In nearly all studies of premixed flames, the number of metal atoms passing through the flame per unit time is constant, since the nebulization rate is held constant. The normal method of adjusting the oxidant-to-fuel ratio in flame spectrometric experiments is to maintain a constant flow rate for the nebulizing gas and vary the flow rate of the other gas to adjust the oxidant-to-fuel ratio. This method, however, results in a changing total flow rate and therefore in a changing sample concentration in the flame. In hydrocarbon flames, the range of oxidant-to-fuel ratios is typically small and the results of measurements in these flames are probably not significantly biased by small changes in the total flow

rate. In hydrogen flames, on the other hand, an extremely wide range of oxidant-to-fuel ratios can be examined, and the results can be highly distorted unless a constant total flow rate is maintained. The degree of distortion which may be generated is illustrated for Zn in Figure 10. The left-hand portion of this figure shows the response surface resulting from the use of a changing total flow rate. The hydrogen flow rate was held constant at 35 l/min (the minimum required to prevent flashback) and the oxygen flow rate was varied from 0 to 19.2 l/min. The other side of this figure illustrated the corresponding surface obtained, as were all the response surfaces discussed below, by maintaining a constant total flow rate of 50 l/min. The error introduced by failure to maintain a constant total flow rate through the burner is evident without a detailed analysis of the response surfaces.

The formation of free atoms in flames from aerosol droplets can be discussed in terms of three basic steps: evaporation of the solvent, vaporization of the desolvated salt particle, and dissociation of metal containing compounds (51). Once free atoms are formed, there are three other processes

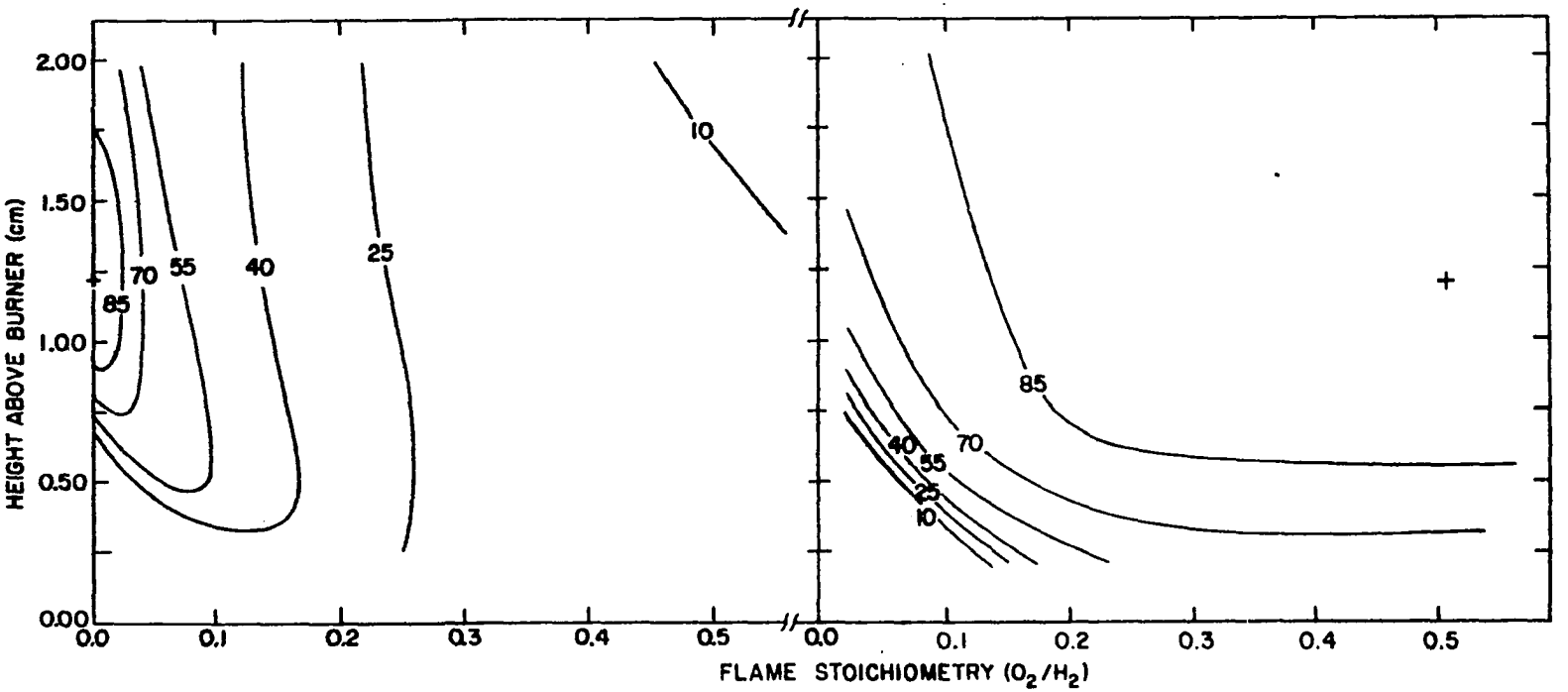

Figure 10. Zn absorbance response surfaces obtained using changing (left) and constant (right) total flow rates

which may reduce atomic number densities (concentrations) in the flame. These are: formation of compounds, ionization, and dilution of the flame gases by air entrained from the atmosphere. All of these processes may occur either sequentially or simultaneously so that it is often difficult to assess their relative importance. Of particular importance is the major role played by the formation of metal monoxides in the atomization process, a subject which has been extensively investigated and interpreted (52,53). A definitive appraisal of the analytical potential of the premixed oxygen-hydrogen flame should therefore include observations on a broad list of elements possessing a range of metal-monoxide (MO) stabilities, as well as other selected properties such as excitation potentials of their spectral lines. The elements selected for study reflect these requirements. In Table 6, these elements are classified, according to the shapes of the shapes of their response surfaces, into 3 groups containing elements whose MO dissociation energies are $\leq$ 4.1 eV (Group I), 4.2 - 5.4 eV (Group II), and $\geq$ 6.4 eV (Group III). The response surfaces of Fe, Ba, and Al were exceptional, so that these elements could not be assigned to any of the above groups.

The absorption and emission response surfaces of Ag shown

Table 6. Properties of the elements and spectral lines examined

	Element	Wavelength (A)	Excitation potential (eV)	Monoxide dissociation energy (eV)
Group I	Na	5890.0	2.11[a]	-
	Ag	3280.7	3.78	2.0[b]
	Zn	2138.6]	5.79	2.8
	Cd	2288.0	5.42	<3.8
	Pb	2170.0	5.71	3.9
	Mg	2852.1	4.34	4.1
	Cu	3247.5	3.82	4.1
	Fe	3719.9	3.33	4.3
Group II	Sr	4607.3	2.69	4.2
	Ca	4226.7	2.93	4.3
	Cr	4254.4	2.91	4.4
	Sn	2246.0	5.52	5.4
	Al	3961.5	3.14	4.6
	Ba	5535.5	2.24	5.8
Group III	V	4379.2	3.13	6.4
	Ti	3642.7	3.42	7.2

[a]Excitation potentials were calculated from those in (54).

[b]Monoxide dissociation energies are the values recommended by Gaydon (55).

in Figure 11 are representative of all the elements in Group I. Since the shapes of these and the other response surfaces discussed below reflect the sensitivities of free atom emission and absorbance to temperature as well as O_2/H_2 and Ht, an effective interpretation requires a mental convolution of

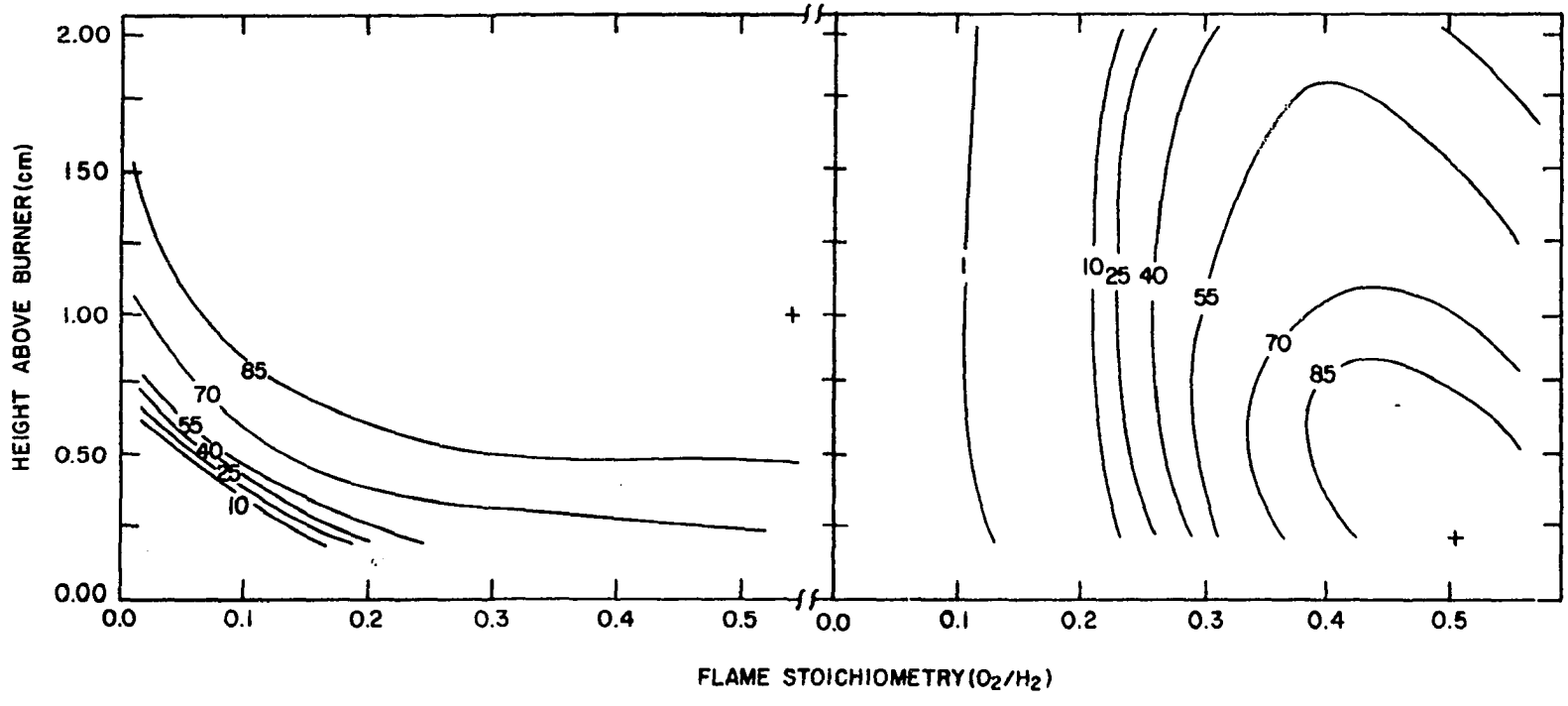

Figure 11. Experimental response surfaces of Ag (10 g/ml) absorbance (left) and emission intensity (right)

the response surface of temperature (Figure 4) with those of atomic emission and absorbance. Referring first to the absorbance plot, it is seen that the highest absorbance, and thus the highest free atom number density, of Ag occurs at O_2/H_2 = 0.55 and at a height of 1.0 cm. The progressive increase in absorbance from 0.25 cm to 0.5 cm above the burner suggests that solvent evaporation and/or solute vaporization are rapidly increasing the concentration of Ag in this part of the flame. This conclusion is consistent with the continuing decrease in absorbance as O_2/H_2 decreases to less than 0.05; temperature also decreases with O_2/H_2 so that solute vaporization rates should be lower, and more time (greater height) should be required for maximal atomization. The fact that maximal absorbance occurs at O_2/H_2 = 0.55 and Ht = 1.0 cm does not, however, imply that solute vaporization is complete at this point. Increasing dilution of the flame gases by entrained air with increasing height may, in fact, cancel increases in free atom populations brought about by more complete atomization. In the relatively flat region of the Ag absorbance response surface, i.e. at Ht < 0.5 cm and oxidant-to-fuel ratios between 0.3 and 0.55, the rates of solute vaporization and dilution appear to be comparable since the

absorbance of Ag is relatively independent of observation site. Absorbance values generally reflect free atom number densities, but because of the large range of oxygen-hydrogen flame temperatures, the absorbance values for Ag as well as for the other elements discussed below, are biased by the dependence of the Doppler halfwidth of the absorption line on temperature. The fact that several elements with very different atomic weights have nearly identical response surfaces suggests that the bias is slight, however. The absorbance of Ag is also relatively independent of O_2/H_2, and therefore of the partial pressure of atomic oxygen in the flame, within the flat region described above. Since the monoxides of all the elements in Group I are relatively unstable, free atom formation for these elements is probably almost complete regardless of the flame environment.

The response surface of Ag emission intensity illustrates the exponential dependence of intensity on temperature. The temperature and Ag emission plots (Figures 4 and 11 respectively) display nearly identical shapes and the points of maximum intensity and temperature correspond exactly.

The Ca absorbance and emission intensity response surfaces shown in Figure 12 are typical of the elements in Table 6 which have MO dissociation energies between 4.2 and 5.4 eV

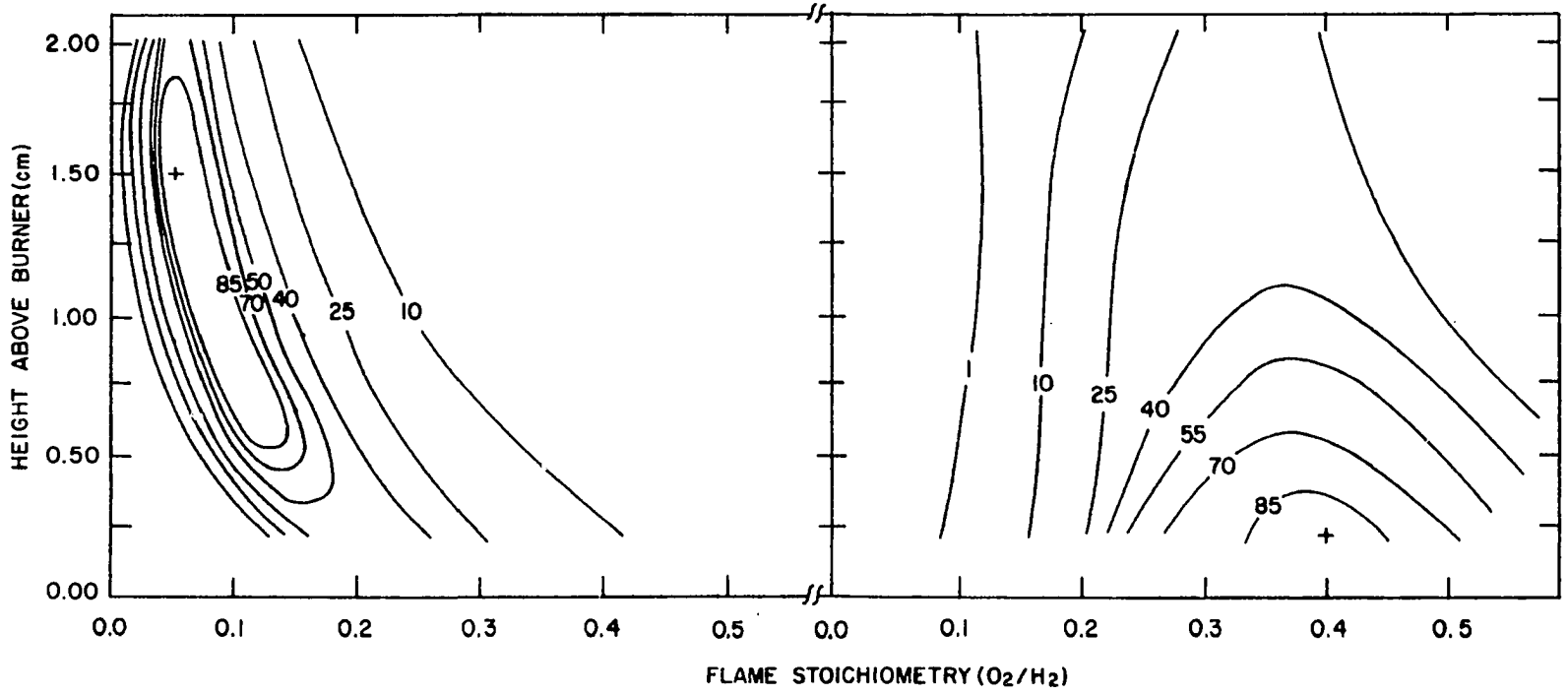

Figure 12. Experimental response surfaces of Ca (10μg/ml) absorbance (left) and emission intensity (right)

(Group II). In contrast to the behavior of Ag and the other elements in Group I, the highest absorbance and consequently the highest free atom number density of Ca is found in the very fuel-rich flame (O_2/H_2 = 0.05) and there is a precipitous drop in absorbance as O_2/H_2 increases to 0.50. Comparison of the response surfaces of temperature (Figure 4), Ca absorbance, and Ag absorbance indicates that the oxygen concentration in the flame and not temperature is of prime importance in the atomization of the elements in Group II. The fact that an oxidant-to-fuel ratio of 0.05 produces maximal atomization of these elements even though the temperature of this flame is only about 1700 K (compared with ~2500 K for the air-acetylene flame (38)) suggests that the oxygen concentration at this point must be very low indeed.

Although the absorbance response surfaces for Ag and Ca are very different, the corresponding emission plots are quite similar, again reflecting the sensitivity of the observed intensity to the flame temperature. The main difference in the emission response surfaces of Ag and Ca is the shift of maximal Ca intensity to a slightly lower oxidant-to-fuel ratio (from 0.55 to 0.40). It is logical to assign this shift to the rapid increase in the Ca free atom partial pressure, although the lower excitation potential of the Ca line

(relative to the Ag line) may be a contributing factor.

Titanium and vanadium, the elements assigned to Group III, both have MO dissociation energies greater than 6 eV. Neither of these elements could be observed in the premixed oxygen-hydrogen flame in either emission or absorption. Evidently a combination of flame composition and temperature suitable for the atomization of these elements does not exist in this flame.

As mentioned earlier, the behavior of Fe, Ba and Al did not correspond with any of the other metals discussed above. The shape of the Fe absorbance response surface is intermediate between those of the elements in Groups I and II. Like Ca, Fe exhibits maximal absorbance in the very fuel-rich flame ($O_2/H_2 = 0.10$), but the decrease in Fe absorbance with increasing O_2/H_2 is less pronounced; the absorbance at $O_2/H_2 = 0.50$ is ~40% of the maximum value. The emission response surface for Fe, as well as those for Ba and Al discussed below, again reflect the convolution of the absorbance and temperature response surfaces.

The shapes of the response surfaces for the Group I and II elements appear to be primarily determined by a single atomization process (solute vaporization and compound formation respectively). A combination of several factors, how-

ever, seems to be responsible for the shapes of the corresponding response surfaces for Ba, which has an MO dissociation energy between those of the elements in Groups II and III, and a relatively low ionization potential (5.2 eV (54)). The Ba response surfaces in Figure 13 are somewhat similar to those of the elements in Group II, but maximal Ba absorbance occurs lower in a less fuel-rich flame than does the corresponding Ca maximum. The flame environments at the points of Ba and Ca absorbance are quite different. The partial pressure of atomic oxygen in the flame and the flame temperature are both higher at the oxidant-to-fuel ratio producing maximal Ba absorbance. The temperature increase should enhance the solute vaporization rate, which would cause the absorbance maximum to occur lower in the flame for Ba than for Ca. The higher temperature should also augment the degree of Ba ionization, which would reduce the atomization efficiency for this element and probably gives rise to the rapid decrease in Ba absorbance with increasing O_2/H_2 and temperature. The higher atomic oxygen partial pressure and temperature should both affect the dissociation of BaO. Higher temperatures increase the equilibrium constants for dissociation reactions of the form:

$$MO \rightleftharpoons M + O$$

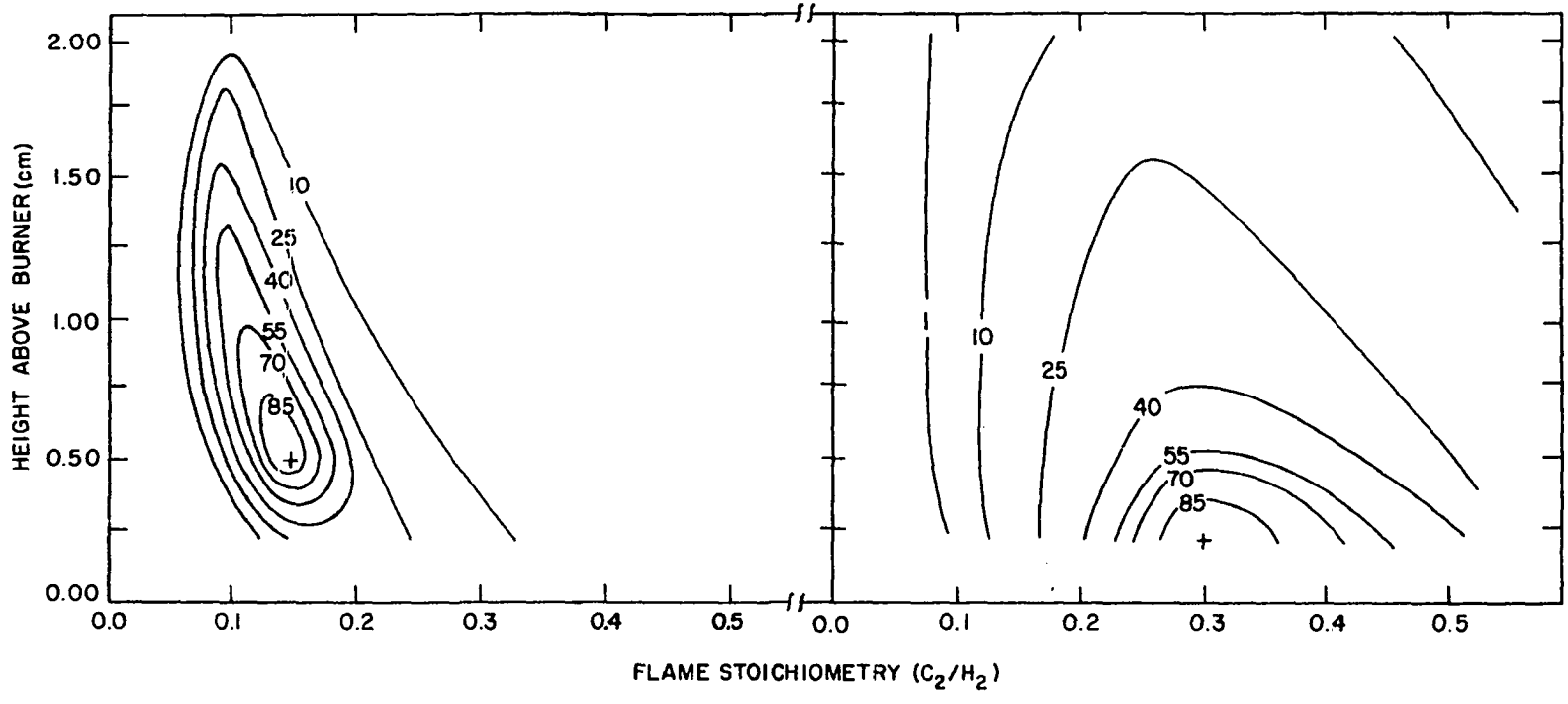

Figure 13. Experimental response surfaces of Ba (100μg/ml) absorbance (left) and emission intensity (right)

while the increase in the partial pressure of atomic oxygen favors the formation of the monoxide.

The experimental results suggest that the increase in the equilibrium constant predominates for Ba, while the effect of increased oxygen partial pressure is most important for Ca and the other elements in Group II. A solution containing 100 μg Ba/ml was required to produce the Ba absorbance response surface whereas only a 10 μg Ca/ml solution was necessary to obtain the Ca surfaces. Allowing for the difference in the atomic weights of these elements, this indicates that the atomization efficiency was somewhat lower for Ba than for Ca. This result is consistent with the relatively high dissociation energy of BaO and the relatively low ionization potential of Ba.

The Al emission intensity response surface in Figure 14 is somewhat similar to those discussed above, but the Al absorbance response surface does not resemble those of any of the other elements in Table 6. Maximal absorbance for Al occurs lower, in a less fuel-rich flame than for either Ba or Ca, and the shape of the Al surface is also unique. The maximum emission intensity and maximum absorbance observed for Al were both very weak, supporting the conclusion of Rasmuson (56) that the dissociation energy for AlO recommended by

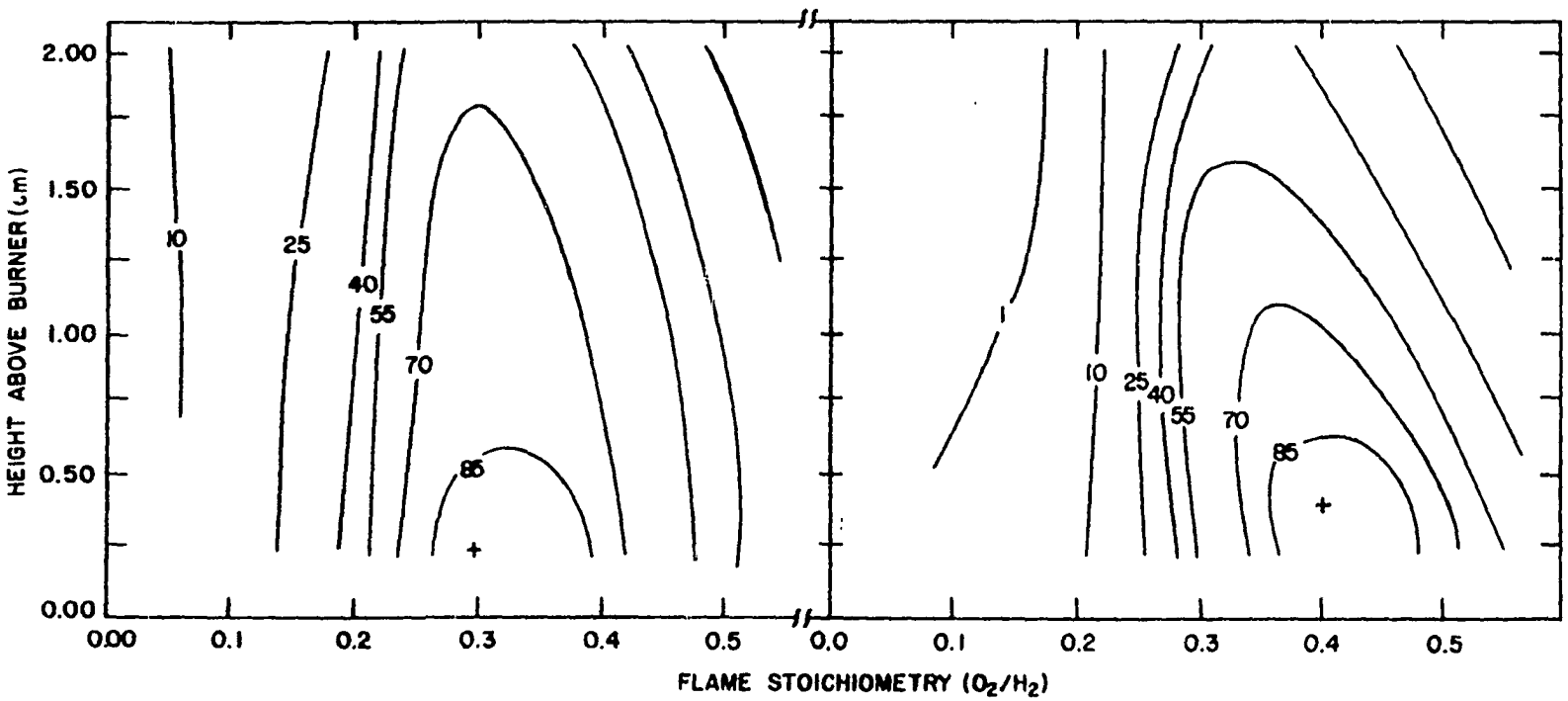

Figure 14. Experimental response surfaces of Al (10,000 µg/ml) absorbance (left) and emission intensity (right)

Gaydon (55) is too low. The free atom fraction calculated by Rasmuson for Al in the nitrous oxide-acetylene flame and the results of this study are both more consistent with the highest value (5.9 eV) in the range of AlO dissociation energies reported by Gaydon (55). It is interesting to note that the higher value was determined by a flame method. Since Al emission and absorbance were very weak, highly concentrated solutions (10,000 μg Al/ml) were required to obtain the response surfaces in Figure 14. Concentrated solutions produce desolvated salt particles in the flame with a larger average size than those produced by more dilute solutions. These larger particles vaporize more slowly and less completely than do smaller ones, as reflected by the slow decrease in Al emission intensity and absorbance with increasing height above the burner. The location of the Al absorbance maximum, then, probably reflects a compromise between the high temperature required for solute vaporization and the flame environment required for maximal production of free Al atoms. The location of the Al absorbance maximum indicates that the solute vaporization effect predominates. This conclusion is supported by many reports of the solute vaporization difficulties associated with samples containing Al (57).

The response surfaces described above illustrate that widely different experimental conditions may be required to produce maximal emission intensity and absorbance for some elements. In addition, these plots indicate the extreme dependence of emission intensity and absorbance on O_2/H_2 and Ht, and reflect the need for careful selection of these parameters prior to the performance of an analysis by flame emission or atomic absorption spectroscopy.

Analytical measurements

Two criteria were employed in the evaluation of the analytical utility of the premixed oxygen-hydrogen flame. The first criterion was the relative magnitude of detection limits for 14 representative elements in the oxygen-hydrogen flame and other flames commonly used in flame spectroscopy. The second criterion was the extent and severity of solute vaporization interferences.

Detection limits The utility of any technique for determining trace impurities depends ultimately upon the lowest concentrations that can be detected with statistical certainty, i.e. the detection limits that can be obtained using the method. In flame spectroscopy, detection limits are most commonly defined (58,59) as that concentration of metal in

solution (μg/ml) which, when aspirated into the flame, produces a signal equal to twice the standard deviation in the background fluctuation. Kaiser (60), however, has shown from statistical considerations, that signals equal to three, rather than two times the standard deviation in the background fluctuation best represent the actual ability to detect the presence of an element. Slack and Fassel (61) have confirmed this conclusion experimentally.

The elements and lines used to prepare the response surfaces discussed in the previous section were also employed in the study of detection limits so that the location of the maximum point on each surface could be correlated with the site at which the maximum signal to-noise ratio was found and the corresponding detection limit was determined. Detection limits are also reported for the line producing the lowest detection limit, however. In both emission and absorption, detection limits were determined using the non-scanning technique commonly employed in atomic absorption spectroscopy.

The lowest (best) absorption detection limits for all the elements examined, except Al, were observed in the very fuel-rich flame ($0.05 \leq O_2H_2 \leq 0.15$), at vertical positions in the flame between 0.75 and 1.00 cm above the burner. This was not

surprising since, in this region of the response surfaces, all the elements except Al absorbed strongly and the flame background noise was minimal (see Figures 8 and 9). Al was exceptional because the absorption of this element was highly localized about the maximum value of O_2/H_2 = 0.30 and Ht = 0.25 cm. The lowest detection limit for Al was actually found at a point 0.75 cm above the site of maximum absorption.

In emission, the best detection limits were observed higher in a more fuel-rich flame than the corresponding emission maxima because the noise level decreased at points higher in the flame and at lower oxidant-to-fuel ratios. All of the lowest detection limits were observed at O_2/H_2 values between 0.30 and 0.45 and at points in the flame between 0.25 and 1.00 cm above the burner.

A summary of detection limits measured in the oxygen-hydrogen flame in this study and similar values reported in the literature for the air-acetylene and nitrous oxide-acetylene flames, in both emission and absorption, is found in Table 7. For a definitive comparison of detection limits in different flames, it is essential to establish whether a bias exists between the values measured in the present investigation and those reported in the literature. For example, the

Table 7. Detection limits

Element	Monoxide dissociation energy (eV)	Line (Å)	Atomic absorption detection limits (g/ml) O_2-H_2	N_2O-C_2H_2	Air-C_2H_2	Flame emission detection limits (g/ml) O_2-H_2	N_2O-C_2H_2	Air-C_2H_2
Ag	2.0[a]	3280.7	0.06	0.005[b]		0.05	0.02[c]	
Al	4.6	3961.5	350.			4.0	0.005[d]	
		3092.8		0.1				
Ba	5.8	5535.5	0.3[d]	0.05[d]		0.08[d]	0.001[d]	
Ca	4.3	4226.7	0.02[d]		0.002	0.002[d]	0.0001[d]	
Cd	<3.8	3261.1					2.0	
		2288.0	0.03		0.005	5.0		
Cr	4.4	4254.4	0.2					
		3578.7	0.05		0.005			

[a]Monoxide dissociation energies were taken from Gaydon (55).

[b]Atomic absorption detection limits in the N_2O-C_2H_2 and air-C_2H_2 flames were taken from Slavin (62).

[c]Flame emission detection limits in the N_2O-C_2H_2 and air-C_2H_2 flames were taken from Koirtyohann and Pickett (58).

[d]KCl added to suppress ionization.

Table 7. (Continued)

Element	Monoxide dissociation energy (eV)	Line (Å)	Atomic absorption detection limits (g/ml) O_2-H_2	N_2O-C_2H_2	Air-C_2H_2	Flame emission detection limits (g/ml) O_2-H_2	N_2O-C_2H_2	Air-C_2H_2
Cu	4.1	3274.0					0.01	
		3247.5	0.09		0.005	0.04		
Fe	4.3	3719.9	0.8			0.2	0.05	
		2483.3	0.06		0.005			
Mg	4.1	2852.1	0.04		0.0003	0.7	0.005	
Na	-	5890.0	0.001		0.002	0.00007		0.0005[d]
Sn	5.4	2246.0	0.6		0.06			
Sr	4.2	4607.3	0.4[d]		0.01	0.02[d]	0.0001[d]	
Zn	2.8	2138.6	0.03		0.002			

large difference between the absorption detection limits measured in the air-acetylene flame by Slavin (62) and those determined in the oxygen-hydrogen flame in this study are inconsistent with the low noise level of the oxygen-hydrogen flame. Table 8 shows that detection limits measured in this study in the air-acetylene and nitrous oxide-acetylene flames are factors of 5 to 20 higher than those reported by Slavin (62). On the other hand, emission detection limits obtained in this study for the nitrous oxide-acetylene flame agreed within factors of 3 to 5 with those determined by Pickett and Koirtyohann (58). Thus an objective comparison of the emission detection limits can be made directly, whereas the absorption detection limits in the air-acetylene and nitrous oxide-acetylene flames should be increased by approximately a factor of 10 to be compared with those determined in the oxygen-hydrogen flame.

The data in Table 7 may now be used to determine whether the premixed oxygen-hydrogen flame provides competitive advantages over the other flames commonly employed in analytical spectroscopy. Several general conclusions can be made. Comparison of the absorption detection limits in the air-acetylene and oxygen-hydrogen flames, for elements which form

Table 8. Comparison of atomic absorption detection limits determined in this study with those of Slavin (62)

Element	Wavelength (Å)	Flame	Detection limits (μg/ml) This study	Slavin
Ca	4226.7	N_2O-C_2H_2	0.009	0.002
Ba	5535.5	"	0.2	0.05
Al	3092.7	"	0.5	0.1
Ti	3642.7	"	4.0	0.2
Cr	3578.7	Air-C_2H_2	0.05	0.005
Fe	2483.3	"	0.06	0.005

relatively unstable monoxides, indicates that the power of detection of these flames are comparable in atomic absorption analyses. Mg falls in this group; the vastly superior absorption detection limit for this element in the air-acetylene flame no doubt can be attributed to the high OH background absorption in the oxygen-hydrogen flame. Elements which form stable monoxides are generally determined in the nitrous oxide-acetylene flame. Comparison of the absorption detection limits for these and other elements in the nitrous oxide-acetylene and oxygen-hydrogen flames reveals that the nitrous oxide-acetylene flame offers greater powers of detection than the oxygen-hydrogen flame. The marginal equivalency of the absorption detection limits for Ba in these two flames is probably due more to the low spectral noise level in the premixed oxygen-hydrogen flame than to comparable atomization

efficiencies for Ba in these two flames.

The relative atomization efficiencies of the nitrous oxide-acetylene and oxygen-hydrogen flames are also reflected by the emission detection limits for elements (Al, Ba, Ca, and Sr) which form stable monoxides and/or hydroxides in flames. These elements all showed superior detection limits in the nitrous oxide-acetylene flame. The emission detection limit for Mg is inferior in the oxygen-hydrogen flame due to spectral coincidence of the Mg line and an OH band component. The fact that Ag, Cd, Cr, Cu, Fe, and Na all have emission detection limits in the oxygen-hydrogen flame equivalent or superior to those in the nitrous oxide-acetylene flame is somewhat surprising because the temperature of the oxygen-hydrogen flame in which these detection limits were measured is approximately 200 K lower than that of the fuel-rich nitrous oxide-acetylene flame. The spectral noise level of the premixed oxygen-hydrogen flame is, however, at least an order of magnitude lower than the noise level of the nitrous oxide-acetylene flame in most regions of the spectrum. This fact is evidently responsible for the equivalence of emission detection limits in these flames.

Skogerboe *et al*. (49) have obtained detection limits of

less than 50 μg/ml for many refractory elements (elements which form very stable monoxides) in a turbulent oxygen-hydrogen flame by using organic rather than aqueous solutions. Their results suggested that the use of organic solvents might improve the detection limits for these elements in the premixed oxygen-hydrogen flame. Results of a preliminary investigation of three refractory elements in ethanol solutions (Table 9) indicated that detection limits in this flame were indeed reduced, but not to the degree observed by Skogerboe et al. The modest improvement in the detection limits for Al was almost certainly due to increased efficiency in nebulizing and evaporating the organic solvent. Titanium and vanadium did not absorb when solutions in either solvent were aspirated into the flame, but both elements emitted when organic solvents are used. The lowest detection limits for Ti and V were found in the primary reaction zone of a fuel-rich flame (O_2/H_2 = 0.20). Ti emitted only under these conditions, but V also emitted at higher oxidant-to-fuel ratios and at points slightly higher in the flame. The fact that Ti and V absorption could not be observed in the premixed oxygen-hydrogen flame indicates that few free, ground state atoms of these elements exist in this flame. The observation of Ti and V

Table 9. Detection limits in the premixed oxygen-hydrogen flame using aqueous and ethanolic solvents

Element	Atomic absorption detection limits (μg/ml)		Flame emission detection limits (μg/ml)	
	H_2O	C_2H_5OH	H_2O	C_2H_5OH
Al	350.	100.	4.	0.8
V	>1000.	>1000.	>1000.	94.
Ti	>1000.	>1000.	>1000.	57.

emission in the primary reaction zone of the oxygen-hydrogen flame suggests, therefore, that excited Ti and V atoms were produced through some non-thermal process which occurs primarily in this zone. The differences in the detection limits determined in the premixed flame and those determined by Skogerboe *et al*. may be due to the difference in burners, since primary combustion occurs throughout the turbulent flame produced by the burners of the type used by Skogerboe *et al*. (Beckman, total consumption type, Beckman Instrument Company, Fullerton, Calif.). Thus the effect of organic solvents may be more widely distributed and enhanced in these flames. The use of organic solvents, then, does not significantly increase the analytical utility of the premixed oxygen-hydrogen flame.

Solute vaporization interferences Constituents in a sample other than those being determined (concomitants) may affect the rate at which the residual aerosol particles are vaporized in the flame. If the vaporization rate is decreased by concomitants, a "chemical" or solute vaporization interference occurs and the absorbance and emission intensity are depressed. The most widely documented examples of solute vaporization interferences are the depression effects observed on Ca emission and absorbance by increasing concentrations of H_3PO_4 or Al concomitants.

The interference of H_3PO_4 on the emission intensity of Ca, observed under experimental conditions approximately the same as those used to determine the emission detection limit for Ca, is illustrated by the upper curve in Figure 15. This curve is quite different from the Ca-PO_4^{-3} interference curves obtained in other flames. In the air-acetylene flame, for example, the Ca intensity generally decreases linearly with increasing PO_4^{-3} concentration to a particular value of PO_4^{-3}/Ca and then remains constant with further increases in the concentration of PO_4^{-3}. This behavior has been widely attributed to the formation of a Ca-PO_4^{-3} compound (51). The emission intensity of Ca in the premixed oxygen-hydrogen flame,

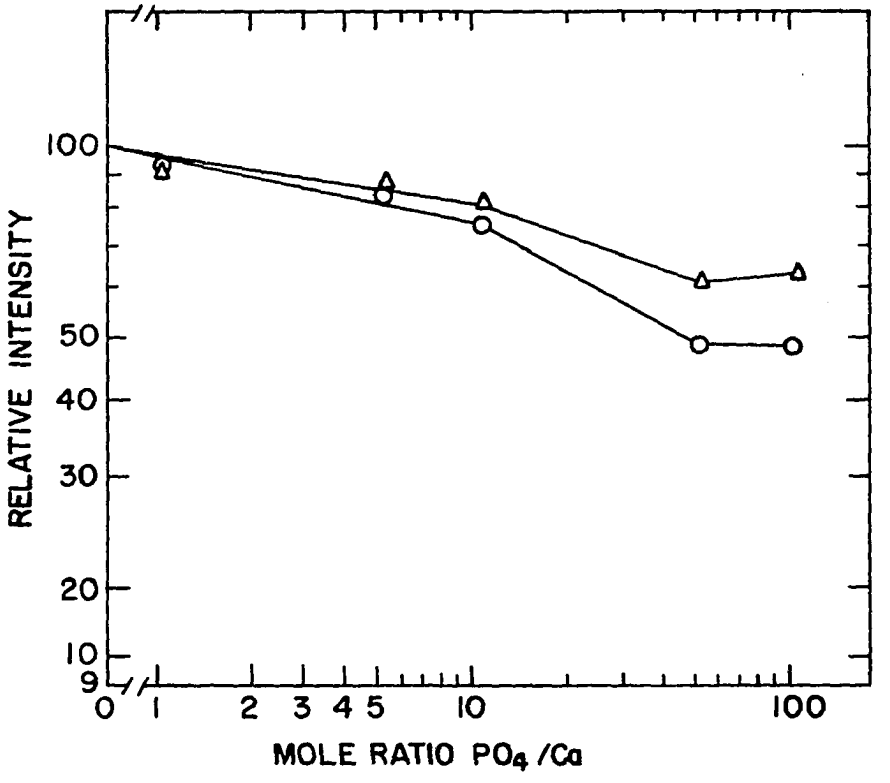

Figure 15. The interference of PO_4^{-3} on the emission intensity of Ca (20 µg/ml) O_2/H_2 = 0.30 Ht = 0.4 cm
Δ - solutions containing only $Ca(ClO_4)_2$ and H_3PO_4
O - solutions containing 1000 µgK/ml as well as $Ca(ClO_4)_2$ and H_3PO_4

however, decreases with increasing PO_4^{-3} concentrations up to a mole ratio (PO_4^{-3}/Ca) of 50/1 and then increases. The solution aspiration rate remained constant for all the solutions used to construct this curve, so nebulization effects are not responsible for its shape. Instead, the Ca-PO_4^{-3} interference curve in Figure 15 appears to be the result of a "bulk matrix effect" (51). Interferences of this type are caused by high total solids concentrations in the sample solution, which results in large desolvated aerosol particles and a low solute vaporization rate. Bulk matrix effects are generally characterized by steadily decreasing analyte emission intensity (and absorbance) with increasing concomitant concentrations above a threshold value. This threshold value is apparently quite low in the oxygen-hydrogen flame for Ca-PO_4^{-3} matrices indicating that solute vaporization of these mixtures is very inefficient in this flame. The increase in Ca emission intensity at high H_3PO_4 concentrations has also been observed in the surface-mixed oxygen-hydrogen and oxygen-acetylene flames (57). The lower curve in Figure 15, which was obtained using solutions containing 1000 µgK/ml (added as KCl) as well as 20 µgCa/ml and varying concentrations of H_3PO_4, illustrates that additional concomitants further reduce

the emission intensity of Ca, as they should if the interference is a bulk matrix effect. Since the interference of H_3PO_4 on Ca in the oxygen-hydrogen flame appears to be comparable to other bulk matrix effects, it should be possible to reduce the interference by sampling the Ca emission at points higher in a hotter, less fuel-rich flame, although this change would also reduce the Ca signal-to-noise ratio.

The interference of Al on the emission intensity of Ca, studied using the same experimental conditions employed for the examination of the PO_4^{-3} interference, is illustrated by the upper curve in Figure 16. Since Ca and Al both have relatively low and nearly equal ionization potentials, this curve reflects an ionization effect as well as the solute vaporization interference. The ionization effect can best be understood by considering the following two reactions:

$$Ca \rightleftharpoons Ca^{+} + e^{-}$$

$$Al \rightleftharpoons Al^{+} + e^{-}$$

As the ratio of Al/Ca increases the electron pressure in the flame increases and the ionization of Ca is suppressed according to the law of mass action. Thus, the concentration of Ca free atoms in the flame increases as a result of the ionization effect. This increase, however, is offset by the solute

Figure 16. The interference of Al on the emission intensity of Ca (20 μg/ml), O_2/H_2 = 0.30, Ht = 0.4 cm

Δ - solutions containing only $Ca(ClO_4)_2$ and $Al(ClO_4)_3$

O - solutions containing 1000 μgK/ml (as KCl) as well as $Ca(ClO_4)_2$ and $Al(ClO_4)_3$

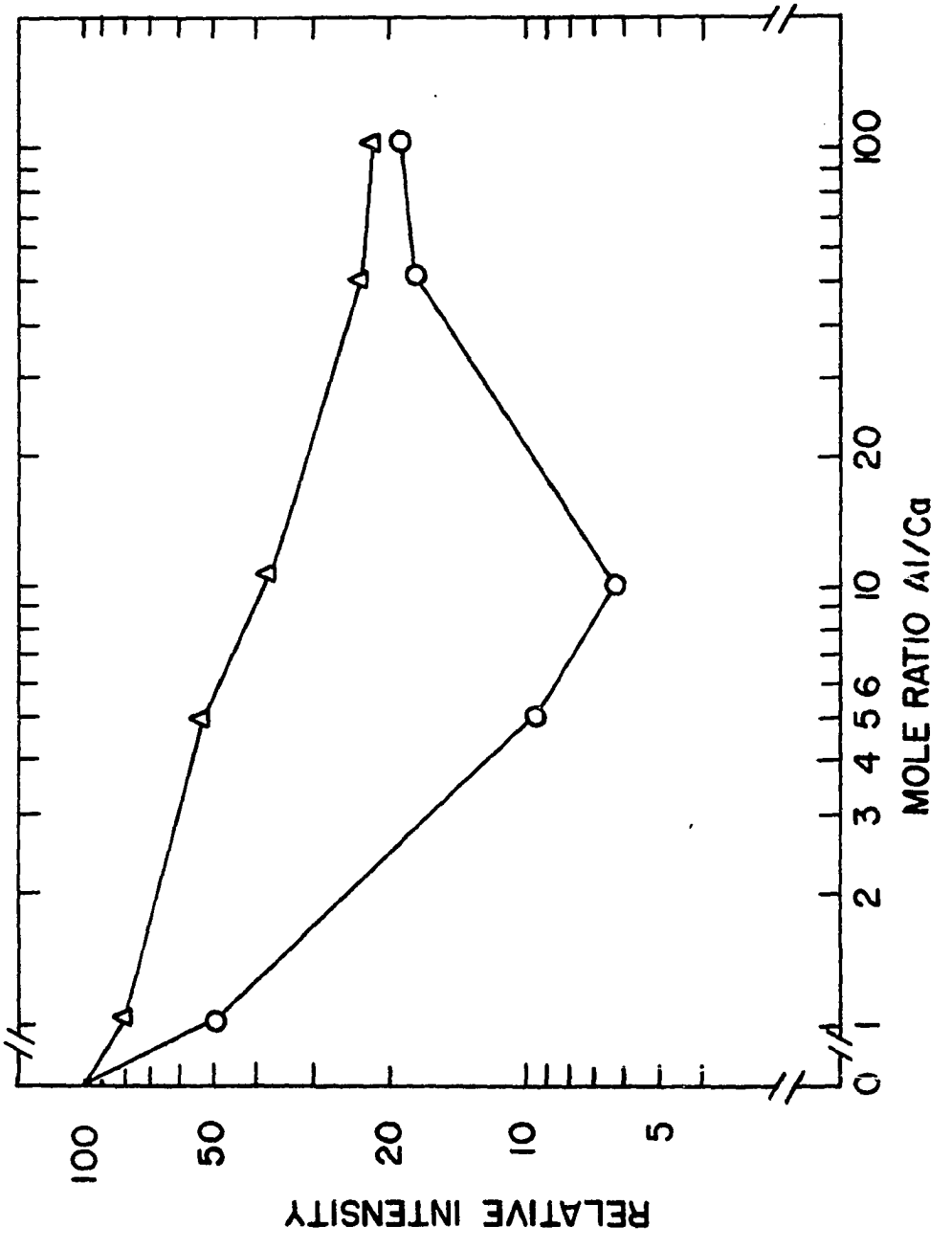
RELATIVE INTENSITY
100
50
20
10
5
0
1
2
3
4
5
6
10
20
100
MOLE RATIO Al/Ca

vaporization interference which reduces the concentration of Ca free atoms in the flame. The lower curve in Figure 16 is the result obtained when the ionization effect is eliminated by suppressing the ionization of both Al and Ca with 1000 μgK/ml added to each of the solutions used to prepare the interference curve. Any KCl matrix effect will be eliminated when the Ca intensities are normalized. This curve illustrates that the emission intensity of Ca is reduced by almost 95% at a mole ratio (Al/Ca) of 10/1, a very serious interference. At mole ratios (Al/Ca) greater than 10/1, however, the effect of Al on Ca decreases. This phenomenon is quite puzzling. Willis et al. (50) observed the same behavior for these elements, but they offered no explanation for it. That the interference curve in Figure 16 reflects the Ca free atom number density and not an excitation effect was confirmed by atomic absorption measurements. The interference of Al on Ca cannot be eliminated by optimizing the experimental conditions. Further study is needed to elucidate the mechanism of this interference.

The severity and temperature dependence of bulk matrix solute vaporization interferences in the premixed oxygen-hydrogen flame are illustrated in Figure 17 by the effect of KCl on the emission intensity and absorbance of Ca, measured

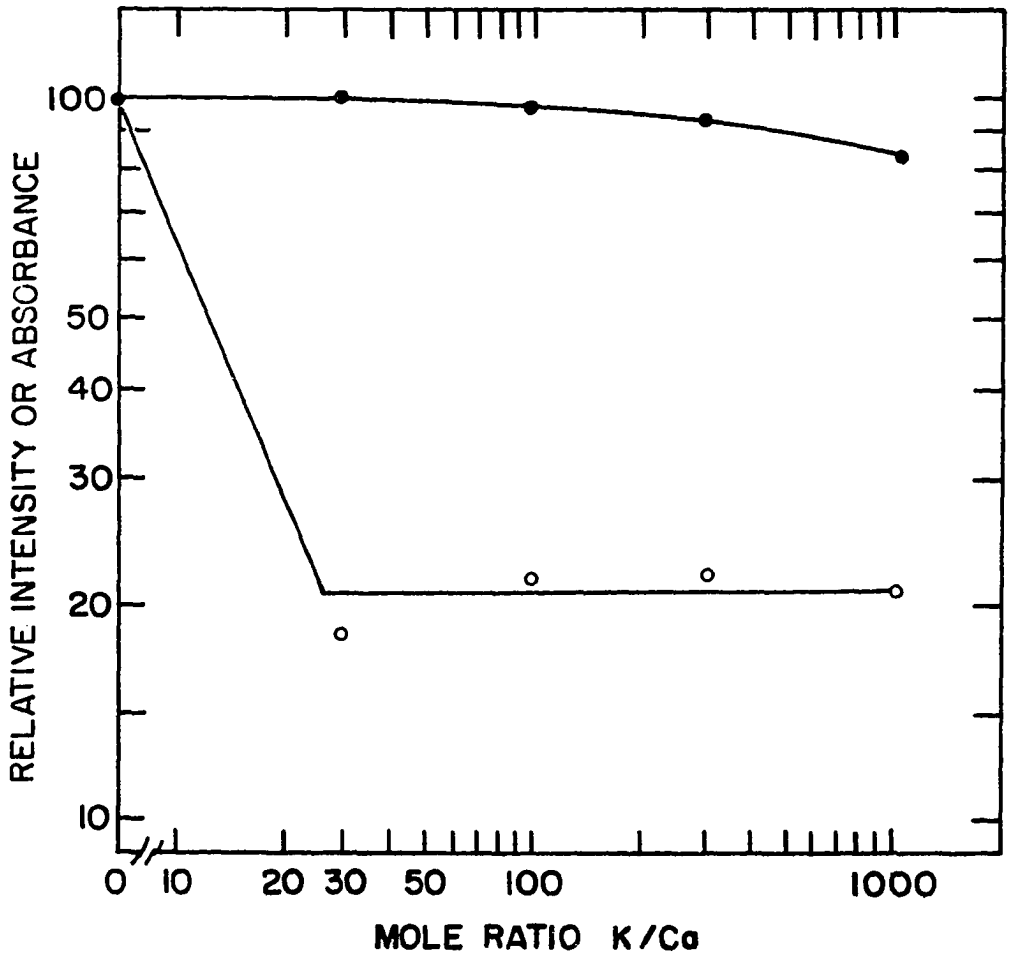

Figure 17. The effect of KCl on the emission intensity and absorbance of Ca (10 μg/ml)
● - Ca emission intensity, O_2/H_2 = 0.40, Ht = 0.25 cm
o - Ca absorbance, O_2/H_2 = 0.05, Ht = 1.25 cm

for the optimal experimental conditions in each mode. The lower curve in this figure shows the interference in absorption at O_2/H_2 = 0.05 and Ht = 1.25 cm, which represents the experimental conditions for maximal Ca atom formation. This curve reveals that even low concentrations of KCl cause large decreases in Ca absorbance. The severity of this interference in absorption is undoubtedly due to the low flame temperature (~1700 K) at this stoichiometry and height. Because concentrations of KCl and other simple salts within the range indicated in Figure 17 cause no interference in the other flames commonly employed in analytical spectroscopy, it is reasonable to assume that many other concomitants cause similar interferences in the cool, very fuel-rich oxygen-hydrogen flame. The upper curve in Figure 17 shows the effect of KCl on Ca at the oxidant-to-fuel ratio (0.40) and height (0.25 cm), which represent the experimental conditions giving maximal emission intensity for this element. In this instance, increasing concentrations of KCl affect both the ionization and solute vaporization of Ca in the hot (~2900 K), slightly fuel-rich flame. Apparently, these two effects cancel each other.

The data in Figures 15 to 17 indicate that the analytical utility of the premixed oxygen-hydrogen flame is severely

limited by the occurrence of serious solute vaporization interferences, particularly in the cool, very fuel-rich flame required for maximal dissociation of even moderately stable metal monoxides. This conclusion is supported by a comparison of the nitrous oxide-acetylene and oxygen-hydrogen flames. In the former, the interference of KCl is not observed and the interferences of H_3PO_4 and Al on Ca can be completely eliminated, in the range of mole ratios indicated in Figures 15 and 16, by the proper selection of experimental conditions (63,64).

Summary and conclusions

Studies of detection limits in the premixed oxygen-hydrogen flame reveal that this flame, despite its high maximum temperature (2950 K) offers few advantages as an atomization cell for flame spectroscopy. Powers of detection in the oxygen-hydrogen and air-acetylene flames are comparable, but detection limits in the oxygen-hydrogen flame are, in general, inferior to those determined in the nitrous oxide-acetylene flame. The equivalency of emission detection limits for several elements in the nitrous oxide-acetylene and oxygen-hydrogen flames is attributable to the extraordinarily low spectral noise level of the latter, in most regions of the

spectrum. Atomization of elements with even moderately stable monoxides is maximal in the cool, very fuel rich oxygen-hydrogen flame, but atomization efficiencies for these elements are severely limited by solute vaporization interferences that occur in this flame.

The use of experimental response surfaces for studying atomic absorption and emission indicates that this method is useful for interpreting the spectroscopic behavior of elements as well as for selecting the optimum conditions for performing an analysis. Experimentally determined response surfaces should also be useful in the design and interpretation of many other experiments in which only two variables are significantly interrelated.

THEORETICAL FLAME MODEL

Introduction

The experimental results discussed above revealed that the premixed, carbon-rich[1] nitrous oxide-acetylene flame is vastly superior to the premixed oxygen-hydrogen flame as an atomization cell, even though its maximum temperature is only 150 K higher. The environmental factors responsible for the superior atomization efficiency exhibited by the carbon-rich nitrous oxide-acetylene flame have been identified both experimentally and theoretically by Rasmuson (56). In view of the success of Rasmuson's model in correlating experimental observations with calculated free atom fractions for elements in the nitrous oxide-acetylene flame, it is of interest to make a similar comparison for the premixed oxygen-hydrogen flame.

Equilibrium in flames

Calculation of the composition of a flame is based on the assumption that thermodynamic equilibrium exists in the portion of the flame considered. Thermodynamic equilibrium exists in a flame when a unique temperature describes the distribution

[1] A carbon-rich flame is a fuel-rich flame which contains appreciable concentrations of carbon containing species such as C_n, CH and CN (56).

of energy among internal and external degrees of freedom of the flame constituents, their ionization and dissociation, and the radiation density in the flame (35). True thermodynamic equilibrium cannot exist in flames because mass, heat, and radiation are continuously transported from the flame. Under certain conditions, however, transfer of energy between translational, vibrational, and electronic modes is more rapid than the transport of energy from the flame. A unique temperature then describes the distribution of energy among these modes, and "local thermodynamic equilibrium" exists. When the concentrations of flame constituents are related by the mass action law, "concentration equilibrium" is said to exist. Because of the occurrence of temperature gradients, the concepts of local thermodynamic equilibrium and concentration equilibrium are meaningful only within small portions of the flame.

Combustion processes

In this context, it is important to examine whether concentration equilibrium exists in the burnt gas region of the premixed oxygen-hydrogen flame. Since the burnt gas region lies immediately downstream from the primary reaction zone, the degree of concentration equilibrium in the former is primarily determined by the combustion processes occurring in

latter. There is now general agreement (4,65-68) that reactions 1-3, operating primarily in the forward direction, play

1. $H + O_2 \rightleftharpoons OH + O$
2. $O + H_2 \rightleftharpoons OH + H$
3. $H_2 + OH \rightleftharpoons H_2O + H$

an important role in the primary reaction zone. As the gases exit the primary reaction zone the reverse processes become increasingly important and the radical recombination reactions 4 to 7 occur. These reactions all include a third, unidenti-

4. $H + H + X \rightarrow H_2 + X$
5. $H + OH + X \rightarrow H_2O + X$
6. $O + O + X \rightarrow O_2 + X$
7. $O + H + X \rightarrow OH + X$

fied species which must be involved in order to conserve momentum. The relative importance of reactions 4 to 7 depends upon the oxidant-to-fuel ratio, but all are highly exothermic and they produce the high temperatures observed in these flames. Combustion mechanisms proposed for clean hydrogen flames do not involve ionized species, a conclusion supported experimentally by Green and Sugden (69).

Concentration equilibrium in premixed oxygen-hydrogen flames

The bimolecular free radical exchange reactions, 1-3, are very fast in both the forward and reverse directions. The

radical recombination reactions, 4-7, on the other hand, are slow in the forward direction because they are termolecular, and in the reverse direction because the activation energies are high (65). Therefore, in the primary reaction zone and for some distance into the burnt gas region, free radical concentrations may exceed their equilibrium values. Since the production of free radicals in the primary reaction zone is relatively independent of temperature while the equilibrium radical concentrations are highly temperature dependent (65), the degree of nonequilibrium is a function of the flame temperature. In flames having temperatures in excess of 2400 K, the concentrations of radicals leaving the primary reaction zone closely approximate their equilibrium values (70). For homogeneous oxygen-hydrogen flames having temperatures greater than 2400 K, the assumption of concentration equilibrium is probably quite valid. This temperature range ($T \geq 2400$ K) includes the stoichiometric and moderately fuel-rich flames.

Very fuel rich oxygen-hydrogen flames, however, may have temperatures considerably less than 2400 K, and the concentrations of radicals entering the burnt gas region in these flames may exceed their equilibrium values by as much as several orders of magnitude (70,71). The lack of free radical equilibrium precludes the calculation of the actual partial

pressures of many species in the very fuel-rich oxygen-hydrogen flame. Fortunately, certain types of reactions are not affected by a lack of free radical equilibrium. Reactions which do not involve free radicals, for example, are not affected because the concentrations of the major flame constituents (H_2 and H_2O) are not appreciably influenced by radical nonequilibrium.

Bulewicz et al. (70) have shown that reactions involving free radicals as both reactants and products are also unaffected by a lack of radical equilibrium. These authors emphasized that reactions 1-3 are very rapid in both the forward and reverse directions. Thus, after ~1 μsec (i.e. as the gases enter the burnt gas region) these rates become equal. Under these conditions, the concentrations of free radicals are interrelated by equilibrium relationships even when they are in excess of their equilibrium values. Schott (72) and Dixon-Lewis (73) have confirmed this conclusion experimentally. The reduction of a metal monoxide in flames is an example of this type of reaction. Two reactions are thought to be primarily responsible for the reduction of a metal monoxide in hydrogen flames (74):

8. $MO + H_2 \rightleftharpoons M + H_2O$ $\qquad K_8 = \dfrac{[M][H_2O]}{[MO][H_2]}$

9. $MO + H \rightleftharpoons M + OH$ $\qquad K_9 = \dfrac{[M][OH]}{[MO][H]}$

where K_8 and K_9 are thermodynamic equilibrium constants. If reaction 8, which contains no radicals, predominates, the reactants and products can be related through the equilibrium constant K_8. If reaction 9, which does contain radicals, predominates, the reactants and products can still be related by K_9 because partial equilibrium exists. The existence of partial equilibrium implies that:

$$K_3 = \frac{[H_2O][H]_a}{[H_2][OH]_a} \qquad [\ ]_a \text{ denotes actual partial pressure}$$

By definition, however,

$$K_3 = \frac{[H_2O][H]_e}{[H_2][OH]_e} \qquad [\ ]_e \text{ denotes equilibrium partial pressure}$$

Thus:

$$\frac{[OH]_e}{[H]_e} = \frac{[OH]_a}{[H]_a}$$

and

$$K_9 = \frac{[M][OH]_e}{[MO][H]_e}$$

The partial pressures of metals and their monoxides are related by the equilibrium constant expression K_9, even when the radical concentrations exceed their equilibrium values. Furthermore, if the reaction mechanism eliminates the effects of nonequilibrium radical concentrations, the equilibrium

constant for any reaction involving M and MO can be used to relate the partial pressures of these species.

Reactions such as 10, on the other hand, are affected by

10. $LiOH + H \rightleftharpoons Li + H_2O$

a lack of radical equilibrium since they contain radicals on only one side of the reaction. Bulewicz et al. (70) have used the fact that reaction 10 reflects the supraequilibrium concentration of hydrogen radicals to measure this quantity.

Procedure

Calculation of the flame composition

Several investigators have calculated the composition of the air-hydrogen flame (34,65). A comprehensive calculation of the composition of the premixed oxygen-hydrogen flame, however, has not been made. The method of Rasmuson (56), which is a modified, computerized version of the procedure described by Gaydon and Wolfhard (34), was used to construct a thermodynamic model of the oxygen-hydrogen flame. The reader is referred to (34) and (56) for a thorough treatment of this method. Briefly, the model is based on the assumption that local thermodynamic equilibrium exists in a closed system containing a definite oxygen-to-hydrogen ratio and temperature. The procedure entails solving a set of simultaneous equations

involving the mass action expressions and the conservation of mass and pressure, for the partial pressures of the significant flame species. Since these equations are, in general, nonlinear and difficult to solve exactly, an iterative technique is used. The constituents considered were O, O_2, OH, H_2O, and H_2, and H. Other, unknown, species may be present in the flame, but if so, their concentrations are probably so low that they exert a negligible influence on the results of the calculation.

Thermodynamic data for the natural flame species as well as for the metals discussed below and their compounds were taken from the latest JANAF tables (75). Measured, rather than adiabatically calculated flame temperatures were used so that the calculated atomization efficiencies approximate the actual values as closely as possible. The experimental facilities and procedures employed for the measurement of flame temperatures were identical to those described previously.

Atomization efficiencies

The atomization efficiency for a metal in a flame is generally expressed as a free atom fraction, β (76), which is defined as the concentration of free neutral atoms (C_n) divided by the sum of the concentrations of all species containing the

metal in the flame volume included in the angle of acceptance of the spectrometer (C_t):

$$\beta = \frac{C_n}{C_t} .$$

All significant metal containing species in the flame must be considered in order to calculate β. However, reaction mechanisms involving many metal containing species contain free radicals only as reactants or only as products (see reaction 10). Concentrations of metal containing species involved in mechanisms of this type are affected by free radical nonequilibrium and thus cannot be accurately calculated in the cool ($T < 2400$ K), very fuel-rich oxygen-hydrogen flame. For many elements, their monoxides are the only molecules formed to a significant degree at the relevant flame temperature. Since the reaction mechanisms proposed for the reduction of metal monoxides were shown above to be independent of free radical nonequilibrium, calculated metal-to-metal monoxide ratios (M/MO) may be employed as a reliable indicator of atomization efficiency for these elements. If other compounds are formed, this estimate of β is the maximum value.

Once the partial pressures of the natural flame species have been determined, calculation of M/MO is straightforward. Free energy functions (77) for the metals, their monoxides,

and O were used to calculate ΔG^{o} for monoxide dissociation reactions having the form:

$$MO \rightleftharpoons M + O \qquad K = \frac{[M][O]}{[MO]}$$

Using the thermodynamic relationship:

$$\Delta G^{o} = - RT\ln K$$

equilibrium constants for each of the monoxide dissociation reactions were then calculated at each oxidant-to-fuel ratio (temperature) considered. Finally, metal-to-metal monoxide ratios were determined at these values of O_2/H_2 by dividing the equilibrium constant by the corresponding value for [O], calculated above.

For a variety of reasons, free energy function data in the temperature region of interest was unavailable for many of the metals studied experimentally or their monoxides. For example, data were not available for CaO, SrO, or BaO due to uncertainties in the ground state electronic configurations of these molecules. The selection of elements for study was thus limited to those in Table 10.

Limitations of the flame model

There are two important limitations to the flame model described above. First, it fails to include the effects of air entrained by the flame, a quantity difficult to measure

Table 10. Elements for which M/MO was calculated

Element	Monoxide dissociation energy (eV)
Na	3.1[a]
Fe	4.2
Be	4.6
Ti	7.2

[a]Dissociation energies in this column were taken from (75).

experimentally. The effects of entrained air are to dilute the flame, to lower its temperature, and to increase the partial pressure of oxygen. Since entrained air enters the flame at the edges, and must diffuse to the center, its effects can be minimized by employing temperatures for the calculation that are measured low in the central portion of the flame.

The second limitation of the model is that it includes the tacit assumption that all the sample entering the flame is vaporized before it enters the zone of observation. This assumption is reasonably valid for dilute metal solutions observed at points greater than 0.5 cm above the burner. Thus, to optimize solute vaporization while minimizing the effects of entrained air, temperatures measured at 0.75 cm above the burner were employed in all calculations.

Results and Discussion

Flame composition

The calculated equilibrium composition of the premixed oxygen-hydrogen flame at various oxidant-to-fuel ratios is shown in Figure 18. As discussed above, the partial pressures of O, OH, and H may be several orders of magnitude higher than the values indicated in this figure, at oxidant-to-fuel ratios less than ~0.15. Of primary importance is the partial pressure of atomic oxygen, since this species plays an important role in the dissociation equilibria of metal monoxides. The partial pressures of all oxygen containing species in the oxygen-hydrogen flame decrease steadily with decreasing oxidant-to-fuel ratio, rather than very rapidly at a distinct flame stoichiometry as they do in the premixed nitrous oxide-acetylene flame (56). This indicates that the chemical environment within the oxygen-hydrogen flame changes less dramatically as the flame is made fuel-rich. Nevertheless, profound changes in the environment within this flame do occur. The calculated pressures of O and O_2, for instance, vary over 8 orders of magnitude within the range of oxidant-to-fuel ratios found in Figure 16. Furthermore, the temperature increases from ~1800 K at O_2/H_2 = 0.07 to 2950 K at O_2/H_2 = 0.50.

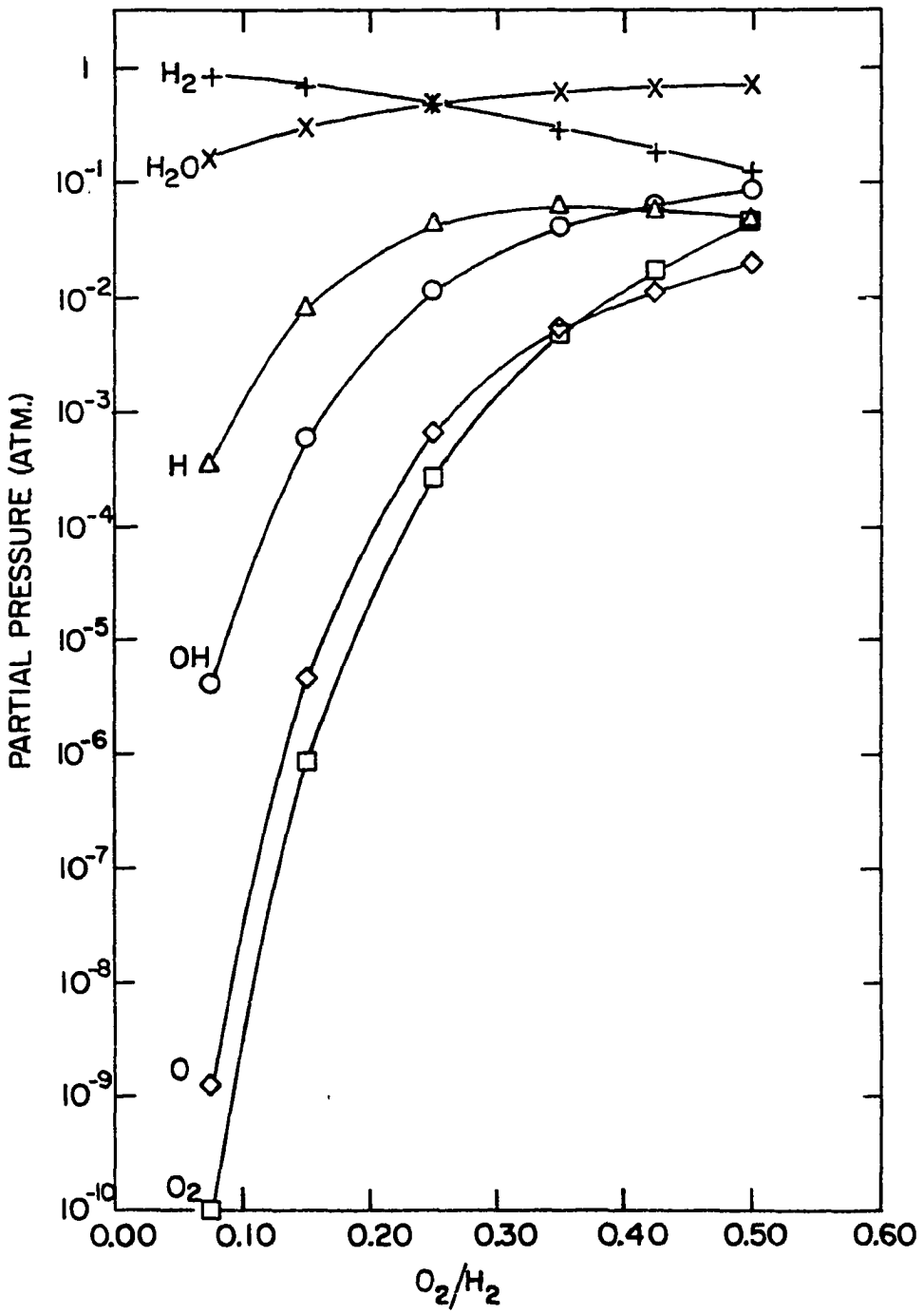

Figure 18. Equilibrium composition of the premixed oxygen-hydrogen flame as a function of oxidant-to-fuel ratio

Atomization efficiencies

The atomization efficiencies for elements in the flame reflect these environmental changes. Metal-to-metal monoxide ratios for 3 of the 4 metals studied, as a function of O_2/H_2, are found in Figure 19. The data illustrated in this figure indicate that the maximum atomization for all elements should be greatest in the very fuel-rich flame. This conclusion confirms the experimental results presented in the previous chapter. Absorption for Na, for example, was found to be nearly independent of O_2/H_2 in the oxygen-hydrogen flame. Maximum Fe absorption was found at $O_2/H_2 = 0.1$ and decreased with increasing O_2/H_2 to 40% of the maximum value at $O_2/H_2 = 0.5$. Absorption by Cr, which has a monoxide dissociation energy close to that for Be, ($D_{oCrO} = 4.4$ eV (55)), also exhibited its absorption maximum in the very fuel-rich flame, but oddly enough, Cr absorption decreased by nearly a factor of 100 as the oxidant-to-fuel ratio is increased to 0.5. The calculated atomization efficiency (M/MO) for Be is probably particularly high because this element forms hydroxides (BeOH and $Be(OH)_2$) as well as a monoxide in flames (56). Beryllium, however, should be illustrative of elements with similar monoxide dissociation energies, that do not form hydroxides.

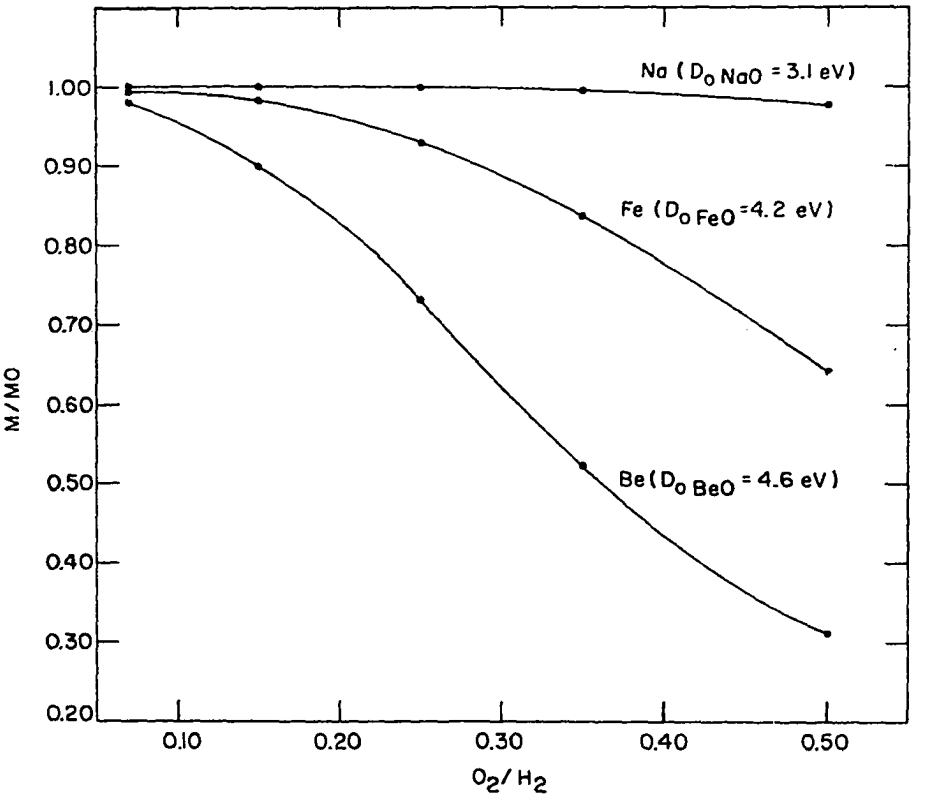

Figure 19. Calculated metal-to-metal monoxide ratios for elements in the premixed oxygen-hydrogen flame as a function of oxidant-to-fuel ratio

Ti (D_{oTiO} = 7.2 eV) is not included in Figure 19 because the maximum calculated value of Ti/TiO was only 6 x 10^{-5} at O_2/H_2 = 0.25. This value is consistent with experimental results since Ti could not be observed spectroscopically, even at concentrations as high as 1000 μgTi/ml.

Comparison of the N_2O-C_2H_2 and O_2-H_2 flames

Since the maximum calculated free atom fraction for Ti in the nitrous oxide-acetylene flame is .33-.49 (56), it is evident that elements that form very stable monoxides are atomized much more efficiently in this flame than in the premixed oxygen-hydrogen flame. The maximum values of M/MO calculated for Na, Fe, and Be in the oxygen-hydrogen flame, on the other hand, are nearly identical to the free atom fractions calculated for these elements in the nitrous oxide-acetylene flame (56). Measured emission and absorption intensities indicate that all the elements examined, except Na, were atomized considerably less efficiently in the oxygen-hydrogen flame. Since the maximum M/MO occurred in the relatively cool (1800 K), very fuel-rich oxygen-hydrogen flame, the most likely explanation for this discrepancy is incomplete solute vaporization. The temperature of the carbon-rich nitrous oxide-acetylene flame is at least 1000 K higher than the temperature

of the very fuel-rich oxygen-hydrogen flame. Fassel and Becker (63) have shown that solute vaporization in this flame is complete in most cases.

Formal thermodynamic calculations illustrate that the very fuel-rich oxygen-hydrogen flame is less efficient than the carbon-rich nitrous oxide-acetylene flame in dissociating stable metal monoxides. In a less formal way, the difference in the reducing powers of these flames can be understood in terms of the relative stabilities of their major products, H_2O (D_{oH_2O} = 5.13 eV (78)) and CO (D_{oCO} = 11.09 eV (55)). Since CO is more stable than H_2O, metal-monoxide reduction reactions producing CO should have larger equilibrium constants than corresponding reactions that produce H_2O. Furthermore, CO is considerably more stable than even the most stable metal monoxide (SiO, D_{oSiO} = 8.2 eV (75). Therefore, dissociation reactions for nearly all metal monoxides in hot hydrocarbon flames (N_2O-C_2H_2 and O_2-C_2H_2) have relatively large equilibrium constants. The dissociation energy of H_2O, on the other hand, is less than or equal to the dissociation energies of many metal monoxides. Equilibrium constants for the dissociation reactions of monoxides more stable than water are thus relatively small. By making the flame more fuel-rich,

the temperature is decreased and the equilibrium constants for monoxide dissociation reactions are reduced. However, the equilibrium partial pressures of atomic oxygen in the cool, very fuel-rich oxygen-hydrogen flame is only 10^{-9} atm or 100 times lower than in the carbon-rich nitrous oxide-acetylene flame. Metals such as Ba, which have monoxide dissociation energies greater than water (D_{oBaO} = 5.8 eV (55)), can thus be appreciably atomized even though the equilibrium constant for the reduction reaction is very small. Elements whose monoxides are relatively unstable with respect to both CO and H_2O, such as Na (D_{oNaO} = 3.1 eV), are easily atomized in all flames and their M/MO ratios are therefore not highly dependent upon the partial pressure of atomic oxygen in the flame.

Practical applications

The results of these calculations indicate that atomization efficiencies for all elements depend upon all the equilibrium conditions that exist for a given set of experimental parameters and not, as implied by Ando et al. (79), on temperature alone. Indeed, the data in Figure 19 indicate that, for the elements in this figure at least, the atomization efficiencies are more dependent upon the partial pressure of oxygen than on the temperature, since the maximum M/MO occurs in the cool, very fuel-rich flame.

BIBLIOGRAPHY

1. Kniseley, R. N., in J. A. Dean and T. C. Rains, eds., Flame Emission and Atomic Absorption Spectrometry, Vol. 1, Marcel Dekker, New York, N.Y., 1969, Chapter 6.

2. Mavrodineanu, R. and H. Boiteux, Flame Spectroscopy, John Wiley and Son, New York, N.Y., 1965.

3. Gilbert, P. T., American Society for Testing and Materials, Special Technical Publications, 269, 73 (1959).

4. Pungor, E., Flame Photometry Theory, Van Nostrand, London, 1967.

5. Dean, J. A., Flame Photometry, McGraw-Hill, New York, N.Y., 1960.

6. Herrmann, R. and C. T. J. Alkemade, Chemical Analysis by Flame Photometry (translated by P. T. Gilbert, Jr.), 2nd rev. ed., Interscience, New York, N.Y., 1963.

7. Ramirez-Munoz, J., Atomic Absorption Spectroscopy, Elsevier, New York, N.Y., 1968.

8. Fiorino, J. A., R. N. Kniseley, and V. A. Fassel, Spectrochim. Acta, 23B, 413 (1968).

9. Willis, J. B., Nature, 207, 715 (1965).

10. Mossotti, V. G. and M. Duggan, Applied Optics, 7, 1325 (1968).

11. Pickett, E. E. and S. R. Koirtyohann, Spectrochim. Acta, 23B, 235 (1968).

12. Willis, J. B., J. O. Rasmuson, R. N. Kniseley, and V. A. Fassel, Spectrochim. Acta, 23B, 725 (1968).

13. Edse, R. and L. R. Lawrence, Jr., Combust. Flame, 13, 479 (1969).

14. Padley, P. J., Trans. Faraday Soc., 56, 449 (1960).

15. Fiorino, J. A., Molecular Absorption and Light Scattering in Flames Employed for Atomic Absorption Spectroscopy, Unpublished Ph.D. thesis, Iowa State University of Science and Technology, Ames, Iowa, 1970.

16. Rains, S. D., Band Absorption by Fuels and Solvents in Atomic Absorption Flames. Paper presented at the Pittsburg Conference on Analytical Chemistry and Applied Spectroscopy, Cleveland, Ohio, March, 1968.

17. Pearse, R. W. and A. G. Gaydon, The Identification of Molecular Spectra, third ed., John Wiley and Son, New York, N.Y., 1963.

18. Gaydon, A. G., The Spectroscopy of Flames, Chapman and Hall, London, 1957.

19. Wolfhard, H. G. and W. G. Parker, Proc. Phys. Soc., A62, 722 (1949).

20. Gaydon, A. G. and H. G. Wolfhard, Proc. Phys. Soc., A65, 2 (1952).

21. Hudson, R. D. and V. L. Carter, J. Opt. Soc. Amer., 58, 1621 (1968).

22. Shuler, K. E., J. Chem. Phys., 19, 888 (1951).

23. Dieke, G. H. and H. M. Crosswhite, Johns Hopkins University Bumblebee Report 87. 1948.

24. Schuler, H. and A. Michel, Z. Naturforsch., 11a, 403 (1956).

25. Schuler, H. and A. Woeldike, Physik Z., 44, 355 (1943).

26. De Galen, L. and J. D. Winefordner, Anal. Chem., 38, 1412 (1966).

27. Lurie, H. H. and G. W. Sherman, Ind. Eng. Chem., 25, 404 (1933).

28. Broida, H. P. and K. E. Shuler, J. Chem. Phys., 27, 933 (1957).

29. Winefordner, J. D., C. T. Mansfield and T. J. Vickers, Anal. Chem., 35, 1611 (1963).

30. De Galen, L. and J. D. Winefordner, J. Quant. Spectrosc. Radiat. Transfer, 7, 703 (1967).

31. Gibson, J. H., W. E. Grossman, and W. D. Cooke, Anal. Chem., 35, 266 (1963).

32. Simon, L., Optik, 19, 621 (1962).

33. Veillon, C. and J. Y. Park, Anal. Chem., 42, 684 (1970).

34. Gaydon, A. G. and H. G. Wolfhard, Flames, Their Structure, Radiation and Temperature, second ed., Chapman and Hall, London, 1960.

35. Snelleman, W., A Flame as a Standard of Temperature, Published Ph.D. thesis, State University of Utrecht, "Bronder-Offset", Rotterdam, Netherlands, 1965.

36. Snelleman, W., Combust. Flame, 11, 453 (1967).

37. Thomas, D. L., Combust. Flame, 12, 541 (1968).

38. Snelleman, W., in J. A. Dean and T. C. Rains, eds., Flame Emission and Atomic Absorption Spectrometry, Vol. 1, Marcel Dekker, New York, N.Y., 1969, Chapter 7.

39. Reif, I., Spectroscopic Temperature Measurements in Non-isothermal flames: Applications to Relative Atomic Transition Probability Determination, Unpublished Ph.D. thesis, Iowa State University of Science and Technology, Ames, Iowa, 1971.

40. de Vos, J. C., Physica, 20, 690 (1954).

41. H. M. Strong and F. P. Bundy, J. Appl. Phys., 25, 1521 (1954).

42. H. M. Strong and F. P. Bundy, J. Appl. Phys., 25, 1527 (1954).

43. H. M. Strong and F. P. Bundy, J. Appl. Phys., 25, 1531 (1954).

44. Box, G. E. P. and K. B. Wilson, J. Roy. Stat. Soc., B13, 1 (1951).

45. Box, G. E., Biometrics, 10, 16 (1954).

46. Skogerboe, R. K., Study of the Optimum Conditions for the Analysis of Some Rare Earths by Atomic Absorption Methods, Unpublished Ph.D. thesis, Montant State College, Bozeman, Montana, 1963.

47. Cellier, K. M. and H. C. T. Stace, Applied, Spectroscopy, 20, 26 (1966).

48. Malakoff, J. L., J. Ramirez-Munoz and W. Z. Scott, Anal. Chim. Acta, 42, 515 (1968).

49. Skogerboe, R. K., A. T. Heybey, and G. H. Morrison, Anal. Chem., 38, 1821 (1966).

50. Willis, J. B., V. A. Fassel, and J. A. Fiorino, Spectrochim. Acta, 24B, 157 (1969).

51. Alkemade, C. TH. J., in J. A. Dean and T. C. Rains, eds., Flame Emission and Atomic Absorption Spectrometry, Vol. 1, Marcel Dekker, New York, N.Y., 1969, Chapter 4.

52. Cowley, T. G., V. A. Fassel, and R. N. Kniseley, Spectrochim. Acta, 23B, 771 (1968).

53. Fassel, V. A., J. O. Rasmuson, T. G. Cowley, and R. N. Kniseley, Spectrochim. Acta, in press.

54. Meggers, W. F., C. H. Corliss and B. F. Scribner, National Bureau of Standards Monograph, 32, Part 1, 1961.

55. Gaydon, A. G., Dissociation Energies and Spectra of Diatomic Molecules, third ed., Chapman and Hall, London, 1968.

56. Rasmuson, J. O., An Experimental and Theoretical Evaluation of the Nitrous Oxide-Acetylene Flame as an Atomiza-

tion Cell for Flame Spectroscopy, Unpublished Ph.D. thesis. Iowa State University of Science and Technology, Ames, Iowa, 1970.

57. Rains, T. C., in J. A. Dean and T. C. Rains, eds., Flame Emission and Atomic Absorption Spectrometry, Vol. 1, Marcel Dekker, New York, N.Y., 1969, Chapter 12.

58. Pickett, E. E. and S. R. Koirtyohann, Anal. Chem., 41 (14), 28A (1969).

59. Fassel, V. A. and D. W. Golightly, Anal. Chem., 39, 466 (1967).

60. Kaiser, H., Anal. Chem., 42 (4), 26A (1970).

61. Slack, R. W. and V. A. Fassel, Iowa State University of Science and Technology, personal communication, 1970.

62. Slavin, W., Atomic Absorption Spectroscopy, Interscience, New York, N.Y., 1968.

63. Fassel, V. A. and D. A. Becker, Anal. Chem., 41, 1522 (1969).

64. Becker, D. A., Chemical Interferences and Ionization in High Temperature Flames, Unpublished Ph.D. thesis. Iowa State University of Science and Technology, Ames, Iowa, 1970.

65. Jenkins, D. R. and T. M. Sugden, in J. A. Dean and T. C. Rains, eds., Flame Emission and Atomic Absorption Spectrometry, Vol. 1, Marcel Dekker, New York, N.Y., 1969, Chapter 5.

66. Dixon-Lewis, G., Proc. Roy. Soc. (London), 298A, 495 (1967).

67. Fenimore, C. P., The International Encyclopedia of Physical Chemistry and Chemical Physics, Macmillan, New York, N.Y., 1964, Topic 19, Vol. 5.

68. Fristrom, R. M. and A. A. Westenberg, Flame Structure, McGraw-Hill, New York, N.Y., 1965.

69. Green, J. A. and T. M. Sugden, in Proceedings of the Ninth Symposium (International) on Combustion, Ithaca, New York, 1962. Academic Press, New York, N.Y., 1963.

70. Bulewicz, E. M., C. G. James, and T. M. Sugden, Proc. Roy. Soc. (London), 235A, 89 (1956).

71. Zeegers, P. T. J., Recombination of Radicals and Related Effects in Flames, Published Ph.D. thesis, State University of Utrecht, "Bronder-Offset", Rotterdam, Netherlands, 1966.

72. Schott, G. D., J. Chem. Phys., 32, 710 (1960).

73. Dixon-Lewis, G., Proc. Roy. Soc. (London), 298A, 495 (1967).

74. Hollander, Tj., Am. Inst. Aeronaut. Astronaut, J., 6, 385 (1968).

75. JANAF Thermochemical Tables, prepared by Dow Chemical Company, Midland, Michigan. Clearinghouse for Federal Scientific and Technical Information, PB-168370, 1966-69.

76. De Galen, L. and J. D. Winefordner, J. Quant. Spectrosc. Radiat. Transfer, 7, 251 (1967).

77. Lewis, G. N. and M. Randall, Thermodynamics, second ed., revised by K. S. Pitzer and L. Brewer, McGraw-Hill, New York, N.Y., 1961.

78. Dwyer, R. J. and O. Oldenberg, J. Chem. Phys., 12, 351 (1944).

79. Ando, A., K. Fuwa and B. L. Vallee, Anal. Chem., 42, 818 (1970).

ACKNOWLEDGMENTS

To Professor V. A. Fassel, I owe my thanks for his guidance, constructive comments and attention to detail during the preparation of this manuscript.

I am also indebted to Mr. R. N. Kniseley for his assistance in solving many technical problems and to Mr. J. O. Rasmuson for many lively and stimulating discussions, as well as assistance in programing. I cannot adequately express my gratitude to my wife Carla. Her love, encouragement and assistance have been of immeasurable value. To Todd, Mike and Matt, I must apologize for the many hours, rightfully theirs, that were consumed by this thesis.